Ultrafast optical excitation of magnetic dynamics in van der Waals magnets: Coherent magnons and BKT dynamics in NiPS₃

Urban F. P. Seifert,[1,2,*] Mengxing Ye ⓘ,[2,*] and Leon Balents ⓘ[2,3]

[1]*Univ Lyon, ENS de Lyon, CNRS, Laboratoire de Physique, 69342 Lyon, France*
[2]*Kavli Institute for Theoretical Physics, University of California, Santa Barbara, California 93106, USA*
[3]*Canadian Institute for Advanced Research, Toronto, Ontario, Canada*

Optical pump-probe experiments carried out in the time domain reveal both the intrinsic low-energy dynamics and its connections to higher-energy excitations in correlated electron systems. In this work, we propose two microscopic mechanisms for the optical generation of coherent magnetic modes in van der Waals magnets, and derive the corresponding effective light-spin interactions: either through pumping atomic orbital excitations resonantly or via a light-induced Floquet spin Hamiltonian, the ground state of the system is driven out of equilibrium. The subsequent long-time relaxational dynamics can then be probed using, e.g., the magneto-optical Kerr effect or transient grating spectroscopy. As an example, we apply our framework to NiPS₃, which is magnetically ordered in the bulk, and is conjectured to realize the XY model in the monolayer limit. Our theory makes explicit how the material's low-energy response depends sensitively on the microscopic details of the light-spin coupling as well as pump fluence, frequency, and polarization. For the case of bulk NiPS₃, we find quantitative agreement with recent experiments [D. Afanasiev *et al.*, Sci. Adv. **7**, eabf3096 (2021)]. We further propose pump-probe experiments for monolayer NiPS₃ and detail how anomalous relaxational behavior may reveal excitations of a (proximate) Berezinskii-Kosterlitz-Thouless phase in a proposed effective XY model.

I. INTRODUCTION

Ultrafast light-matter interaction provides a powerful means to probe and control quantum materials [1–3]. By pumping the system to a nonequilibrium state, the probed relaxation dynamics may reveal intrinsic coherent excitations. Recent advances in the field of ultrafast optics have enabled coherent control of quantum materials through nonthermal pathways, where the quantum coherence in the transition process must be taken into account. While these nonthermal pathways enable more control by the pump polarization, frequency, fluence, etc., they also pose the theoretical challenge of identifying microscopic mechanisms suitable for pumping in a specific setting. Several mechanisms have been explored both experimentally and theoretically to optically excite coherent magnetic excitations [4–6], e.g., through coupling with optically active phonons, or direct coupling with spin excitations. Recent experiments also showed coherent magnetic excitations through pumping in the mid-infrared to near-infrared range, where the light couples to correlated electronic degrees of freedom or atomic excitations.

Moving a step forward towards a *systematic* understanding of the microscopic pathways of optical generation of coherent magnetic excitations, in this study we explore two distinct microscopic mechanisms, one resonant and another nonresonant, through optically pumping atomic orbital excitations and Floquet engineering, respectively.

Our studies are motivated by recent experiments by Afanasiev *et al.* in Ref. [7], which point towards markedly distinct mechanisms of exciting coherent magnons in the same material. Using a pump-probe setup, they find that applying linearly polarized pump beams to the bulk van der Waals magnet NiPS₃ allows one to selectively excite two distinct modes of oscillations in the Faraday rotation of the probe beam as signature of the coupled dynamics of the Néel order parameter and magnetization.

NiPS₃, which belongs to the family transition-metal thiophosphates, has zigzag-antiferromagnetic Néel order in the ground state [8–10]. A single-ion easy-plane anisotropy causes the spins to lie within a plane, with a weaker easy-axis anisotropy due to monoclinic stacking of layers setting an in-plane ordering direction (for the definition of the spin Hamiltonian and modeling of the magnon dynamics we refer the reader to Sec. IV). The low-energy magnon modes of the system thus correspond to pseudo-Goldstone modes. The lowest-energy mode is associated with rotations of the Néel vector against the in-plane easy-axis anisotropy, dubbed f_1 in Ref. [7], while fluctuations of the out-of-plane component give rise to a higher-frequency mode f_2. The former is found to be excited for pump beam energies in a narrow frequency range around 1.0 eV, close to the energy of an atomic orbital transition. However, strikingly, the out-of-plane mode is excited with an almost equal amplitude for a wide range of photon energies from 0.1 up to 0.9 eV. This remarkable difference in the dependence of the excited modes on the driving light's frequency suggests, in the spirit of the discussion above, that two distinct excitation mechanisms are at play.

In this work, we show that the optical pumping of orbital atomic excitations is efficient to drive the resonant f_1 mode. Furthermore, we show that the transient Floquet spin Hamiltonian allows for additional anisotropic terms, which disturb the zigzag ground-state ordering pattern. This can explain the f_2 mode being excited in a transparent energy window. We emphasize that spin-orbit coupling is crucial to optically excite magnetic excitations through electronic transitions.

Both the microscopic mechanisms as well as the theoretical framework to describe the ultrafast excitation process discussed here can be readily generalized to pumping other types of magnetic excitations. As a second example, we hence discuss pumping hydrodynamic modes in the Berezinskii-Kosterlitz-Thouless (BKT) phase and its proximate phases. This may be realized in the monolayer limit of NiPS$_3$, which was found to exhibit a drastic suppression of antiferromagnetic ordering compared with two-layer and bulk samples [11].

Framework

Our methodology in modeling the microscopic excitation mechanism of coherent magnetic excitations in ultrafast pump-probe setups consists in finding an effective microscopic Hamiltonian $\mathcal{H}_{\mathrm{eff}}$ which is active for the duration of the pump in second-order perturbation theory in the electric field of the driving light. Time evolution according to this Hamiltonian takes the system out of equilibrium and thus sets the initial conditions for the subsequent relaxation dynamics according to the equilibrium low-energy equations of motion.

In the case of bulk NiPS$_3$, the homogeneous low-energy excitations consist of two sets of coupled harmonic oscillators

$$\partial_t n_\alpha \sim \chi^{-1} m_\beta - h_{m,\beta}(t), \quad \partial_t m_\beta \sim -\kappa_{n_\alpha} n_\alpha + h_{n,\alpha}(t) \quad (1)$$

for the components of the Néel vector $\boldsymbol{n}$ and the magnetization $\boldsymbol{m}$, with $\alpha = y(z)$ and $\beta = z(y)$ for the in-plane f_1 (out-of-plane f_2) mode when the Néel order is along x. The source terms $h_{m,\beta}$ and $h_{n,\alpha}$ correspond to effective uniform and staggered magnetic fields induced by the pump beam's electric field, and can be obtained by considering the action of $\mathcal{H}_{\mathrm{eff}}$ on the low-energy variables of the system. We note that this approach presupposes that the time evolution induced by the pump pulse is unitary, and thus that the concept of an effective (Hermitian) Hamiltonian is well defined. Interestingly, this assumption is *not* satisfied for driving frequencies which are resonant with a (sharp) atomic transition, as we discuss in Sec. II B. In this case, the initial conditions for the low-energy variables set by the perturbing light can be evaluated directly in a microscopic picture using a generalized (nonunitary) time-evolution operator. Equation (1) nevertheless still holds (with $h_. = 0$) after the pulse.

With an advanced understanding of the microscopic mechanisms governing the excitation of low-energy magnons in conventionally ordered magnetic systems at hand, it is of prime interest to turn to more exotic magnetic phases of matter. Here, ultrafast optical methods may serve as an additional probe into the dynamics of more exotic excitations beyond the linear-response regime. To this end, we study pumping hydrodynamic modes in the BKT phase and its proximate phases.

The general phase diagram of a two-dimensional (2D) magnet with easy-plane anisotropy and hexagonal symmetry consists of two phase transitions at T_{BKT} and T_c, where $T_{\mathrm{BKT}} > T_c$ [12]. Below T_c, the system orders into one of the six degenerate minima selected by the hexagonal anisotropy. Above T_{BKT}, the system is disordered with exponential decaying correlations. At any $T_c < T < T_{\mathrm{BKT}}$, the system exhibits critical algebraic order. Crucially, the pump-induced excitation and subsequent relaxation of spin-wave modes in the (quasi)ordered phases and diffusive spin modes in the disordered phases can be readily modeled using the framework described above: The time evolution according to the effective Hamiltonian which is active during the pump, with the respective light-induced local anisotropies and exchange interactions between the $S = 1$ local moments, then sets the initial conditions for the subsequent low-energy dynamics of the in-plane phase of the Néel order parameter and the out-of-plane magnetization, which are conveniently modeled in terms of a *dual* electromagnetic theory in order to account for the presence of free vortices and bound vortex-antivortex pairs [13].

We emphasize that our framework can be readily applied to other systems with hexagonal symmetry and spin-orbit coupling, with only minor modifications required to account for the possibly distinct crystalline symmetries. Furthermore, coherent magnetic excitations aside from magnon and hydrodynamic modes may be excited within this framework, such as quadrupolar waves proposed in NiGa$_2$S$_4$ [14].

The remainder of the paper is organized as follows. In Sec. II, we discuss single-ion multiplets of a Ni^{2+} ion in appropriate crystal fields and derive electric-field-induced single-ion anisotropies. The modification of (anisotropic) exchange interactions in the pump period is discussed in Sec. III. We then model the long-range magnetic order and the light-induced dynamics of coherent low-energy magnons in bulk NiPS$_3$, using the results of the preceding sections in Sec. IV. In Sec. V, we generalize the framework to pumping hydrodynamic modes in and proximate to the BKT phase.

II. PUMP-INDUCED SINGLE-ION ANISOTROPY

Motivated by the observation in Ref. [7] that the low-energy in-plane mode f_1 in NiPS$_3$ is excited in a rather narrow pump photon energy range which coincides with the energy of the $^3A_{2g} \rightarrow {}^3T_{2g}$ interorbital resonance of a Ni^{2+} ion, we first focus on a single ion in a d^8 configuration in an octahedral crystal field environment (with a small trigonal distortion).

The laser's electric field induces virtual transitions out of the orbital-singlet, spin-triplet ground state to the first excited multiplet. As the latter is split under spin-orbit coupling, we can use time-dependent second-order perturbation theory to derive an effective time evolution in the $S = 1$ ground-state sector which includes light-induced single-ion spin anisotropy terms. Here we emphasize that spin-orbit coupling is a crucial ingredient as it allows the orbital resonance to couple to spin, which ultimately yields transitions between distinct spin states in the ground-state manifold. We further note that within our local approach of considering a single Ni^{2+} ion with octahedral symmetry, all dipole matrix elements between the $^3A_{2g}$ ground-state multiplet and the first excited $^3T_{2g}$ multiplet vanish by the dipole selection rule, as the
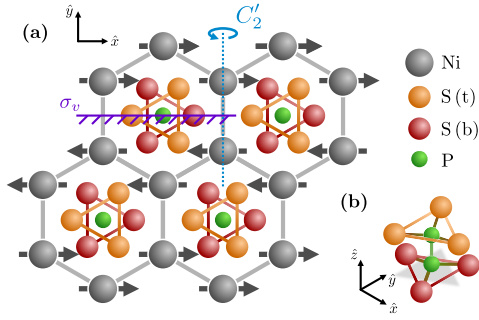
FIG. 1. Schematic visualization of NiPS$_3$ crystal structure. (a) Projection in the $\hat{x}$-$\hat{y}$ plane, where S (t) and S (b) denote sulfur atoms on the top and bottom of a $(P_2S_6)^{4-}$ cluster. The gray arrows indicate the zigzag Néel due to the Ni^{2+} local moments arranged on a honeycomb lattice. The axis for the C_2' symmetry is shown marked light blue, and the vertical mirror plane σ_v in purple. We also show the noncubic crystal field environment (with broken inversion symmetry) for a Ni site. (b) Three-dimensional (isometric projection) illustration of a $(P_2S_6)^{4-}$ cluster.

electric-field-induced dipole operator $r^\alpha \overset{\mathcal{I}}{\to} -r^\alpha$ is odd under inversion $\mathcal{I}$, while A_{2g} and T_{2g} are even under $\mathcal{I}$, such that $\langle A_{2g}|r^\alpha|T_{2g}\rangle = -\langle A_{2g}|r^\alpha|T_{2g}\rangle \equiv 0$. However, this an artifact of the single-ion picture since, in NiPS$_3$, the sites of the Ni^{2+} are not inversion centers as the surrounding S atoms, stemming from the P$_2$S$_6^{4-}$ clusters, break the cubic symmetry, as visible from Fig. 1. In this structure, the symmetry of the Ni sites is hence reduced to D_3. We therefore emulate the inversion-symmetry breaking by constructing a ground-state wave function for the A_2 orbital singlet which contains inversion-odd components due to the hybridization induced by ligand holes on the Ni^{2+}. The induced anisotropy terms take the Néel vector out of equilibrium for the duration of the pump pulse and thus set initial conditions for the subsequent relaxation dynamics governed by the equilibrium equations of motion.

A. Ni^{2+} single-ion multiplets

To set the stage, the Ni^{2+} ion is in the local crystal field environment with D_3 symmetry, which is weakly broken from the cubic symmetry O_h due to trigonal splitting. We note that under an octahedral crystal field the ^3F ground-state multiplet of two unpaired d electrons ($d^8 \simeq d^2$) is split as $^3F \to {}^3A_{2g} + {}^3T_{1g} + {}^3T_{2g}$, with $^3A_{2g}$ constituting the $S = 1$, orbital-singlet ground-state manifold and $^3T_{2g}$ the first excited multiplet. To explicitly construct the corresponding wave functions from the single-particle d-orbital wave functions, it is convenient to choose the single-particle wave functions as eigenstates of the C_3 rotation operator about the [111] axis in the cubic reference frame, where $\omega = e^{i2\pi/3}$ denotes the third root of unity.

The orbital component of the ground state is then given as $|A_{2g}\rangle = \frac{1}{\sqrt{2}}(|e_{\omega^2}\rangle_1 |e_\omega\rangle_2 - |e_\omega\rangle_1 |e_{\omega^2}\rangle_2)$, and the orbital sector of the first excited $^3T_{2g}$ multiplet is spanned by $|T_{2g}, 1\rangle$, $|T_{2g}, \omega\rangle$, and $|T_{2g}, \omega^2\rangle$, with explicit expressions given in Eq. (A4). The energy of the first excited multiplet on top of the ground state is given by $\varepsilon_{T_{2g}} - \varepsilon_{A_{2g}} \equiv \Delta \equiv 10Dq$.

We now discuss the effect spin-orbit coupling $\mathcal{H}_{\text{SOC}} = \lambda \vec{L} \cdot \vec{S}$ perturbatively. As the $^3A_{2g}$ multiplet is an orbital singlet, its threefold degeneracy will only be lifted at higher-order perturbation theory through mixing with the excited levels. Conversely, the degeneracy of the $^3T_{2g}$ multiplet is lifted under spin-orbit coupling at first order in λ. For our purposes, it is convenient to define a fictitious angular momentum $l = 1$ acting on the T_{2g} orbital triplet. An explicit calculation reveals that

$$\mathcal{P}_{T_{2g}} \vec{L} \mathcal{P}_{T_{2g}} = \tfrac{1}{2}\vec{l}, \tag{2}$$

where $\mathcal{P}_{T_{2g}} = \sum_{a=1,\omega,\omega^2} |T_{2g}, a\rangle \langle T_{2g}, a|$ denotes the projection operator into the orbital triplet. At first order in λ, the degeneracy in the first excited multiplet is split with the effective Hamiltonian $\mathcal{H}_{\text{SOC}}^{\text{eff}}$. Introducing the (fictitious) total angular momentum $\vec{J}_{\text{eff}} = \vec{S} + \vec{l}$, the three sectors have quantum numbers $J_{\text{eff}} = 0$, $J_{\text{eff}} = 1$, $J_{\text{eff}} = 2$ and energies $\varepsilon = -\lambda$, $-\lambda/2$, and $\lambda/2$, respectively.

It is convenient to transform spatial coordinates to the trigonal reference frame with an orthogonal matrix W,

$$\begin{pmatrix} x \\ y \\ z \end{pmatrix} \mapsto \begin{pmatrix} \frac{2z-x-y}{\sqrt{6}} \\ \frac{x-y}{\sqrt{2}} \\ \frac{x+y+z}{\sqrt{3}} \end{pmatrix} \equiv W \begin{pmatrix} x \\ y \\ z \end{pmatrix}, \tag{3}$$

such that the quantization axes of spin and fictitious angular momentum operators coincide with the $\hat{z}$ *axis, which is also the axis of the C_3 rotation operation. Note that with this choice of reference frame, the splitting $^3T_{2g} \to {}^3A_1 + {}^3E$ (for $\lambda = 0$) under a trigonal distortion of the crystal field can be accounted for in degenerate perturbation theory through the effective Hamiltonian

$$\mathcal{H}_{\text{tri}}^{\text{eff}} = \delta(l^z)^2. \tag{4}$$

For both $\lambda, \delta \neq 0$ the $^3T_{2g}$ multiplet is split into three doublets and three singlets which carry quantum numbers $S^z + l^z$. However, for simplicity, we take $\delta = 0$ in the present discussion and note that a finite (but small) $\delta \neq 0$ could account for further level splitting and a fine structure of the experimentally observed resonance peaks.

B. Time-dependent perturbation theory

We now employ time-dependent perturbation theory to study how the degeneracy of the $S = 1$, orbital-singlet ground-state sector spanned by $|A_{2g}, S^z = 0, \pm 1\rangle$ is lifted by the perturbing electric field, which induces transitions to the $J_{\text{eff}} = 0, 1, 2$ manifolds arising from spin-orbit splitting of the first excited multiplet. To this end, we consider the perturbing Hamiltonian

$$\mathcal{H}^{\text{E}} = r^\alpha \mathcal{E}_\alpha(\omega)e^{i\omega t} + r^\alpha \mathcal{E}_\alpha^*(\omega)e^{-i\omega t} \tag{5}$$

which yields the time-evolution operator in the interaction picture

$$U_{\text{I}}(t, t_0) = \mathcal{T} e^{-i\int_{t_0}^t \mathcal{H}_{\text{I}}^{\text{E}}(t')dt'}. \tag{6}$$

Expanding to second order and projecting to the $S = 1$ subspace, we find the matrix elements of the effective

time-evolution operator within that subspace as

$$\langle a|U_{\text{eff}}(t, t_0)|b\rangle$$

$$\approx \delta_{ab} - \sum_m \int_{t_0}^{t} dt' \int_{t_0}^{t'} dt'' \langle a|\mathcal{H}_{\text{I}}^{\text{E}}(t')|m\rangle \langle m|\mathcal{H}_{\text{I}}^{\text{E}}(t'')|b\rangle,$$

$$(7)$$

where $|a\rangle \equiv |S^z\rangle$ denote the three states in $S = 1$ ground-state sector and $|m\rangle = |J_{\text{eff}}, J_{\text{eff}}^z\rangle$ are the states in the spin-orbit-split first excited multiplet. Focusing on a pump pulse of length t_p which is switched on at $t_0 = 0$, the temporal integrations can be performed analytically, yielding

$$\langle a|U_{\text{eff}}(t_p, 0)|b\rangle \approx \delta_{ab} + \mathcal{E}_\alpha \mathcal{E}_\beta^* \sum_m \frac{\langle a|r^\alpha|m\rangle \langle m|r^\beta|b\rangle}{i(\omega - \varepsilon_{m0})}$$

$$\times \left[t_p - \frac{e^{i(\omega - \varepsilon_{m0})t_p} - 1}{i(\omega - \varepsilon_{m0})} \right], \qquad (8)$$

where we have kept only the dominant term for $\omega \approx \varepsilon_{m0} > 0$ with $\varepsilon_{m0} = \varepsilon_m - \varepsilon_0$ denoting the energy difference between the ground state and the first excited sector.

In the off-resonant limit, i.e., when $t_p(\omega - \varepsilon_{m0}) \gg 1$ for all m, the second term in the square brackets in (8) tends to 0, and the time-evolution operator can be written in terms of a pump-induced effective (Hermitian) Hamiltonian $U_{\text{I}}(t_p, 0) \approx \mathbb{1} - i\mathcal{H}_{\text{eff}}t_p$, as discussed by Pershan *et al.* in Refs. [15,16].

On the other hand, in the resonant limit $t_p(\omega - \varepsilon_{m0}) \ll 1$ it is seen that the time-evolution operator

$$\langle a|U_{\text{eff}}(t_p, 0)|b\rangle \rightarrow \delta_{ab} - \mathcal{E}_\alpha \mathcal{E}_\beta^* \sum_m \langle a|r^\alpha|m\rangle \langle m|r^\beta|b\rangle \frac{t_p^2}{2} \quad (9)$$

becomes nonunitary, as the ground-state wave function acquires a finite overlap with the excited levels due to real transitions mediated by the perturbation, which is not captured within our approach of projecting to the $S = 1$ states.

Near a resonance, the notion of an effective pump-induced time-independent Hamiltonian thus no longer applies. Instead, we will make use of the time-evolution operator projected to the low-energy subspace to directly compute the pump-induced initial conditions for relaxational low-energy dynamics as described in Sec. IV.

In order to evaluate the time-evolution operator in the $S^z = \pm 1, 0$ basis of the $^3A_{2g}$ ground state, we first note that the equilibrium Hamiltonian $\mathcal{H}_0$ is diagonal following the above

considerations, and has elements

$$\mathcal{H}_0 |A_{2g}, S^z\rangle = 0, \qquad (10)$$

$$\mathcal{H}_0 |J_{\text{eff}}, J_{\text{eff}}^z\rangle = \left(\Delta + \frac{\lambda}{4} J_{\text{eff}}(J_{\text{eff}} + 1) - \lambda \right) |J_{\text{eff}}, J_{\text{eff}}^z\rangle, \quad (11)$$

where $J_{\text{eff}} = 0, 1, 2$. Using the multiplet wave functions constructed in the previous section, however, immediately yields $U_{\text{I}} \approx \mathbb{1}$ as all dipole matrix elements between d orbitals in the nominator of (8) vanish, in apparent contradiction to the experimentally observed orbital resonance. To resolve this inconsistency, we note that recent experimental and first-principles numerical studies [17,18] have recently shown that the Ni ground state contains, in addition to the d^8 configuration, a strong admixture of a $d^9\underline{L}$ configuration, where $\underline{L}$ denotes a ligand p-orbital hole. As the numerical modeling of a Ni-ligand cluster in Ref. [17] finds the hole-doped contribution to the ground-state wave function $|\psi\rangle$ to be actually dominant $|\langle d^9\underline{L}|\psi\rangle|^2 = 0.60$ (compared to $|\langle d^{10}\underline{L}^2|\psi\rangle|^2 = 0.15$ and $|\langle d^8|\psi\rangle|^2 = 0.25$), we in the following consider the ground-state configuration $e_g\underline{L}$ comprised of an e_g and $\underline{L}$ hole. We emphasize that in the case of octahedral symmetry the resulting ground-state wave function is found to be of (approximate) $^3A_{2g}$ symmetry and thus, given the oddness of the dipole operator appearing in the perturbing electric field Hamiltonian $\mathcal{H}_{\text{I}}^{\text{E}}$, all dipole matrix elements for transitions to the first excited multiplet remain forbidden (however, trigonal distortions in the $\underline{L}$ hole may induce an e_u representation at the Ni^{2+} site). Given that in NiPS_3 the Ni are no longer centers of inversion of the NiS_6 clusters, the e_u orbitals due to the ligand hole may hybridize with the e_g deriving from the Ni^{2+} d levels to form an inversion-odd component in the full A_2 orbital-singlet ground state given by

$$|A_2\rangle = \tfrac{1}{2}[|e_\omega\rangle_1 |p_{\omega^2}\rangle_2 + |e_{\omega^2}\rangle_1 |p_\omega\rangle_2 + (1 \leftrightarrow 2)], \qquad (12)$$

where we drop all other contributions which will yield vanishing transition dipole matrix elements.

We are now in a position to evaluate (8) where we take $|A_{2g}, S^z\rangle \rightarrow |A_2\rangle |S^z\rangle$. We consider a pump beam at normal incidence to basal planes of NiPS_3, implying (in the trigonal reference frame) that $\mathcal{E}_z \equiv 0$.

The resulting time-evolution operator U_{eff} for a single Ni^{2+} $S = 1$ moment can then be written in the form (up to constants quadratic in $\mathcal{E}$)

$$U_{\text{eff}}(t_p, 0) = \mathbb{1} + C_{A_1}^z(t_p)\mathcal{E} \cdot \mathcal{E}^*(S^z)^2 + C_{A_2}^z(t_p)(i\mathcal{E} \times \mathcal{E}^*)S^z$$

$$+ C_E^{xy}(t_p)[(\mathcal{E}_x\mathcal{E}_y^* + \mathcal{E}_y\mathcal{E}_x^*)(S^x S^y + S^y S^x) + (\mathcal{E}_x\mathcal{E}_x^* - \mathcal{E}_y\mathcal{E}_y^*)((S^x)^2 - (S^y)^2)]. \qquad (13)$$

Here, we have labeled the coefficients by the irreducible representations of D_3 under which the respective electric field bilinears transform. In general, these coefficients $C_X^\alpha = \text{Re}\, C_X^\alpha + i\, \text{Im}\, C_X^\alpha$ are complex, and become purely imaginary (real) in the off-resonant (resonant) limit. We further stress that these coefficients $C_X^\alpha = C_X^\alpha(t_p)$ depend on the pump

length t_p. For technical details on the derivation of (13), we refer the reader to Appendix A 2.

The first term in (13) corresponds to a light-induced modulation of the single-ion anisotropy normal to the plane of incidence and is proportional to total intensity of the light, implying a polarization-independent result, with the

coefficient

$$C_{A_1}^z = -\frac{i}{24}(2g_0 - 3g_1 + g_2), \quad (14)$$

where $g_j = \frac{1}{\omega - \epsilon_{m_j 0}}[t_p - \frac{e^{i(\omega - \epsilon_{m_j 0})\iota_p} - 1}{i(\omega - \epsilon_{m_j 0})}]$, $j = 0, 1, 2$, with $\epsilon_{m_j 0}$ the energy difference between the ground state and the excited state with $J_{\text{eff}} = j$ in Eq. (11).

The matrix elements of the second term in (13), transforming in the A_2 irreducible representation, are proportional to the chiral intensity $i\mathcal{E} \times \mathcal{E}^* = i\mathcal{E}_\alpha \mathcal{E}_\beta^* \epsilon^{\alpha\beta}$ $(\alpha, \beta = x, y)$ which is finite only for circularly polarized light, and couples to the z component of the local moment. In the off-resonant limit, this term is thus understood as a light-induced Zeeman magnetic field, which lies at the heart of the "inverse Faraday effect" [1,6,16]. The corresponding coefficient reads as

$$C_{A_2}^z = -\frac{i}{24}(2g_0 + 3g_1 - 5g_2). \quad (15)$$

Further, there are two terms in (13) which belong to the two-dimensional E representation of D_3 and are analogous to single-ion anisotropies within the xy plane (which coincides with the crystallographic basal plane). The coefficient reads as

$$C_E^{xy} = \frac{i}{24}(2g_0 - 3g_1 + g_2). \quad (16)$$

An inspection of the symmetry properties of the system reveals that in principle one can consider a second two-dimensional E representation involving the spin bilinears $\{S^x, S^z\}$ and $\{S^y, S^z\}$ which, however, is absent from the $\mathcal{U}_{\text{eff}}$. This follows from a generalized dipole selection rule for the fictitious orbital angular momentum: Noting that the dipole operator at normal incidence only involves x and y components, allowed transitions need to satisfy $\Delta J_{\text{eff}}^z = \pm 1$, where it is understood that $J_{\text{eff}}^z \equiv S^z$ in the A_2 ground state (in which the orbital angular momentum is quenched) and $J_{\text{eff}}^z = l^z + S^z$ in the excited states. It thus follows that matrix elements of $\mathcal{U}_{\text{eff}}$ in the ground-state manifold derived from second-order perturbation theory are either diagonal or need to satisfy $\Delta J_{\text{eff}}^z \equiv \Delta S^z = \pm 2$, which is only facilitated by products of two operators of the type $S^\pm = S^x \pm iS^y$, and thus S^z cannot couple to any off-diagonal spin operators.

We plot the frequency dependency of $C_{A_2}^z$ and C_E^{xy}, which are of relevance to the excitation of spin waves in NiPS$_3$ (see also Sec. IV), informed by realistic microscopic parameters, in Fig. 2. In particular, as we detail in Sec. IV, when pumping with linearly polarized light, only the C_E^{xy} term contributes to the in-plane mode f_1. On the other hand, exciting the out-of-plane mode f_2 requires spin bilinears $\{S^x, S^z\}$ and $\{S^y, S^z\}$, which is absent here due to the generalized dipole selection rule stated above. This explains the experimental observation in Ref. [7] that only the f_1 mode is excited in the narrow resonant frequency range.

III. ANISOTROPIC EXCHANGE INTERACTIONS AND FLOQUET SPIN HAMILTONIAN

Motivated by the observation of low-energy out-of-plane mode f_2 in a broad frequency range transparent in optical absorption, we consider an off-resonant mechanism, where the
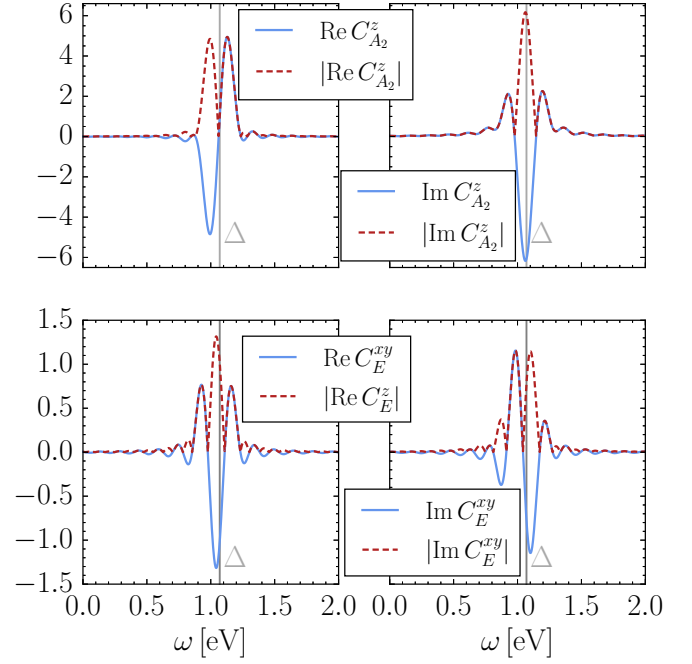

FIG. 2. Plot of the real and imaginary parts of $C_{A_2}^z$ [Eq. (15)] and C_E^{xy} [Eq. (16)] (and their absolute values for comparison with Ref. [7]) as a function of the light's driving frequency. Here, we have taken the crystal field splitting [7] $\Delta = 1.07$ eV and spin-orbit coupling [18] $\lambda = 0.08$ eV, and a boxcar pump profile of 100 fs $\approx$ 41.36 meV. Note, a nonuniform pump pulse will likely lead to a further smearing of the frequency dependence of the observed intensities.

Floquet spin Hamiltonian introduces effective magnetic fields that couple to the slow spin fields $\boldsymbol{n}$, $\boldsymbol{m}$ [see Eq. (1)]. Similar to the orbital-resonance-induced spin transition as discussed in Sec. II, the SOC is essential here for the pump field to induce anisotropic spin interactions, and thus generate an effective staggered field along $\hat{z}$ or $\hat{y}$ which couples to the Néel vector.

To understand the possible spin interaction channels, we first obtain the effective bilinear spin Hamiltonian in equilibrium from a minimal two-orbital Hubbard model on a honeycomb lattice. In particular, we will focus on the anisotropic spin exchanges which require SOC. In equilibrium, these anisotropic terms will modify the spin-wave spectrum, but do not contribute to the effective magnetic fields when the zigzag order is the true ground state. Next, we obtain the corresponding nonequilibrium spin exchange through the Floquet formalism, and identify the effective field up to quadratic order in the pump electric field.

A. Equilibrium spin-exchange interactions

For simplicity, we ignore the ground-state multiplet in $d^9 \underline{L}$ configuration, and restrict to the four states in the d^8 configuration at half-filling in the e_g orbitals for each Ni^{2+}. We will focus only on the nearest-neighbor (NN) and third-nearest-neighbor (TNN) terms, both of which are invariant under the twofold rotation along the bond (C_2'), product of bond inversion (i.e., with the inversion center given by a midpoint of a bond), and mirror with the mirror plane perpendicular

to the bond ($\mathcal{I} \times \sigma_v$), and time reversal (see also Fig. 1 for an illustration of the C_2' axis and mirror plane). We then use the threefold-rotational symmetry about a Ni site and translational symmetries to generate hopping terms for the full lattice.

We hence obtain the general symmetry-allowed tight-binding Hamiltonian within e_g orbitals (ignoring the ligand atoms), which reads as

$$
\mathcal{H}_t = \sum_{\mathbf{r} \in A, \boldsymbol{\delta}_i} \Psi_{\mathbf{r}}^{\dagger} \big[W_{C_3}^{i-1} (w_0 \tau_0 \sigma_0 + w_1 \tau_z \sigma_0 + w_2 \tau_y \sigma_z
$$
$$
+ w_3 \tau_y \sigma_x)(W_{C_3}^{\dagger})^{i-1} \big] \Psi_{\mathbf{r}+\boldsymbol{\delta}_i} + \text{H.c.}, \tag{17}
$$

where $\Psi_{\mathbf{r}} = (e_{\omega,\uparrow}, e_{\omega,\downarrow}, e_{\omega^2,\uparrow}, e_{\omega^2,\downarrow})_{\mathbf{r}}^{\top}$, $\boldsymbol{\delta}_i = \boldsymbol{\delta}_i^{(l)}$ with $i = 1, 2, 3$, denotes the NN ($l = 1$) or TNN ($l = 3$) bonds. $\boldsymbol{\delta}_1$ is along the $\hat{y}$ direction in trigonal coordinate, and $\boldsymbol{\delta}_i = \mathcal{R}_{C_3}^{i-1} \boldsymbol{\delta}_1$. Here, $W_{C_3}, \mathcal{R}_{C_3}$ are the threefold-rotation operations acting on the single-particle fermion operators Ψ and $3d$ spatial vectors, respectively. τ_i, σ_i are identity ($i = 0$) and Pauli matrices ($i = 1, 2, 3$) in the orbital and spin space, respectively. Note that among the hopping integrals denoted as w_μ ($\mu = 0, \dots, 3$), w_2 and w_3 require SOC.

To capture the onsite interactions, for simplicity, we consider only the intraorbital Hubbard repulsion $\mathcal{H}_U = U \sum_{i,\alpha} \hat{n}_{i,\alpha}(\hat{n}_{i,\alpha} - 1)$, where α labels the e_g orbitals. Note that Hund's coupling (J_H) and interorbital Hubbard interaction (U') do not contribute to the exchange coupling at the leading order in J_H, U' because the atoms active in the excited state perturbed by $\mathcal{H}_t$ are occupied by one electron (hole). The effective spin Hamiltonian at half-filling obtained through second-order perturbation theory in $t/U \ll 1$ is given by

$$
\mathcal{H}_{\text{eff}}^{\text{ex}} = -\mathcal{P}_s \mathcal{H}_t \mathcal{P}_d \frac{1}{\mathcal{H}_U} \mathcal{P}_d \mathcal{H}_t \mathcal{P}_s, \tag{18}
$$

where $\mathcal{P}_{s,d}$ are projection operators on the single- and double-electron occupancy space. $\mathcal{H}_{\text{eff}}^{\text{ex}}$ up to a constant is

$$
\mathcal{H}_{\text{eff}}^{\text{ex}} = \sum_{\mathbf{r}, \boldsymbol{\delta}_i} \vec{S}_{\mathbf{r}}^{\top} \Gamma^{\boldsymbol{\delta}_i} \vec{S}_{\mathbf{r}+\boldsymbol{\delta}_i}, \tag{19}
$$

where $\Gamma^{\boldsymbol{\delta}_i} = \mathcal{R}_{C_3}^{i-1} \Gamma^{\boldsymbol{\delta}_1} \mathcal{R}_{C_3}^{\top i-1}$, and

$$
\Gamma^{\boldsymbol{\delta}_1} = \begin{pmatrix} J_l - J_l' + J_l'' & 0 & J_{l,xz} \\ 0 & J_l - J_l' - J_l'' & 0 \\ J_{l,xz} & 0 & J_l + J_l' - J_l'' \end{pmatrix}. \tag{20}
$$

Here, J_l is the lth NN isotropic Heisenberg exchange, $J_l', J_l'', J_{l,xz}$ are the anisotropic spin exchange that requires SOC. Specifically, we find

$$
J_l = \frac{2(w_0^2 + w_1^2)}{U},
$$
$$
J_l' = \frac{-2w_2^2}{U}, \quad J_i'' = \frac{2w_3^2}{U}, \quad J_{l,xz} = \frac{4w_2 w_3}{U}, \tag{21}
$$

with $w_\mu = w_\mu^{(l)}$ denoting the $\mu = 0, \dots, 3$ hopping amplitudes on $l = 1, 3$ nearest-neighbor bonds as introduced in (17).

In passing, we note that there are a few cautions to fully apply the minimal model to NiPS$_3$. *First*, in this consideration, the exchange paths are limited to only between Ni ions. However, in transition-metal trichalcogenide, the ligand atoms play an important role to determine the sign of the exchange interactions. Indeed, the NN Heisenberg term is found to be ferromagnetic [10], which cannot be explained by the antiferromagnetic superexchange presented in Eq. (20). It instead requires considering the superexchange paths through the ligand atoms following the Goodenough-Kanamori approach [8,19]. Similarly, for the TNN spin exchange, the super-superexchange paths are dominant [10,20]. Nevertheless, the current consideration obtains all symmetry-allowed spin-exchange terms and will be taken to derive the Floquet spin Hamiltonian with the right symmetry.

Second, aside from electron hopping w_2, w_3, SOC may also enter into the effective spin Hamiltonian through onsite term $\mathcal{H}_{\text{SOC,onsite}} = \lambda_{\text{SOC}} \sum_i \Psi_i^{\dagger} \tau_y \sigma_z \Psi_i$. However, we note that the ground-state multiplet is an orbital singlet, $\mathcal{H}_{\text{SOC,onsite}}$ does not have nonzero matrix element within the ground-state multiplet manifold. A careful analysis including both $\mathcal{H}_t$ and $\mathcal{H}_{\text{onsite,SOC}}$ indicates that the onsite SOC does not contribute to the anisotropic spin Hamiltonian up to $\frac{w_0^2 \lambda^2}{U^3}$, so will be ignored in further discussions.

B. Floquet spin Hamiltonian

We consider the following periodically driven Hubbard model:

$$
\mathcal{H}_t(t) = \sum_{\langle i,j \rangle} w_{is_1, js_2}^{\alpha \beta} e^{-ie\boldsymbol{A}(t) \cdot \boldsymbol{r}_{ij}} \hat{v}_{i\alpha s_1, j\beta s_2} + \text{H.c.},
$$
$$
\mathcal{H}_U = U \sum_i \hat{n}_{i\alpha}(\hat{n}_{i\alpha} - 1), \tag{22}
$$

where $\boldsymbol{r}_{ij} = \boldsymbol{r}_i - \boldsymbol{r}_j$, and the effects of the pump laser are manifested in the kinetic energy $\mathcal{H}_t(t)$ through the Peierls substitution. For compactness, we have introduced the electron hopping operator $\hat{v}_{i\alpha s, j\beta s'} = e_{i\alpha s}^{\dagger} e_{j\beta s'}$ that denotes the hopping of spin s' orbital β electron at site j to spin s orbital α electron at site i.

Consider the electric field $\vec{E} = \frac{1}{2}(\vec{\mathcal{E}} e^{i\omega t} + \vec{\mathcal{E}}^* e^{-i\omega t})$, the gauge term reads as

$$
e^{-ie\boldsymbol{A}(t) \cdot \boldsymbol{r}_{ij}} = e^{i \frac{\Omega_{ij}}{\omega} \sin(\omega t + \phi_{ij})} = \sum_{n=-\infty}^{n=\infty} e^{in(\omega t + \phi_{ij})} \mathcal{J}_n\left(\frac{\Omega_{ij}}{\omega}\right), \tag{23}
$$

where the "Rabi" frequency of the laser for bond $\langle ij \rangle$ is $\Omega_{ij} = e\sqrt{(\text{Re}\vec{\mathcal{E}} \cdot \boldsymbol{r}_{ij})^2 + (\text{Im}\vec{\mathcal{E}} \cdot \boldsymbol{r}_{ij})^2}$, the phase ϕ_{ij} is determined by $\tan \phi_{ij} = \text{Im}\vec{\mathcal{E}} \cdot \boldsymbol{r}_{ij}/\text{Re}\vec{\mathcal{E}} \cdot \boldsymbol{r}_{ij}$ In the off-resonant limit, i.e., when $|U - n\omega|$ is much greater than the bandwidth of the many-body excited states, we can ignore the heating due to, e.g., doublon decay [21], the Floquet spin Hamiltonian from

the Hubbard model can be expressed as

$$
\mathcal{H}_{\text{eff}}^{\text{ex}} = - \sum_{\langle ij \rangle, n, n'} w_{js_1', is_2'}^{\alpha'\beta'} w_{is_1, js_2}^{\alpha\beta} \mathcal{J}_{n'}\left(\frac{\Omega_{ji}}{\omega}\right) \mathcal{J}_n\left(\frac{\Omega_{ij}}{\omega}\right) e^{i(n+n')\omega t} e^{i(n'\phi_{ji} + n\phi_{ij})} \mathcal{P}_s \hat{v}_{j\alpha's_1', i\beta's_2'} \frac{\mathcal{P}_d}{\mathcal{H}_U + n\omega} \hat{v}_{i\alpha s_1, j\beta s_2} \mathcal{P}_s
$$

$$
\rightarrow - \sum_{\langle ij \rangle, n} w_{js_1', is_2'}^{\alpha'\beta'} w_{is_1, js_2}^{\alpha\beta} \mathcal{J}_n\left(\frac{\Omega_{ji}}{\omega}\right) \mathcal{J}_{-n}\left(\frac{\Omega_{ij}}{\omega}\right) e^{in(\phi_{ji} - \phi_{ij})} \mathcal{P}_s \hat{v}_{j\alpha's_1', i\beta's_2'} \frac{\mathcal{P}_d}{\mathcal{H}_U - n\omega} \hat{v}_{i\alpha s_1, j\beta s_2} \mathcal{P}_s
$$

$$
= - \sum_{\langle ij \rangle, n} w_{js_1', is_2'}^{\alpha'\beta'} w_{is_1, js_2}^{\alpha\beta} \mathcal{J}_n^2\left(\frac{\Omega_{ji}}{\omega}\right) \mathcal{P}_s \hat{v}_{j\alpha's_1', i\beta's_2'} \frac{\mathcal{P}_d}{\mathcal{H}_U - n\omega} \hat{v}_{i\alpha s_1, j\beta s_2} \mathcal{P}_s. \tag{24}
$$

From the first to second line, we have considered only the time-independent effective spin Hamiltonian, and to obtain the last line, we have used $\phi_{ij} = \phi_{ji} + \pi$. Note that compared with the equilibrium spin Hamiltonian, the pump laser only modifies the effective exchange coupling strength of a given bond $\langle ij \rangle$ by a factor $\mathcal{J}_n^2(\frac{\Omega_{ji}}{\omega})\frac{U}{U - n\omega}$. For linearly polarized light, $\Omega_{ij} = e|\text{Re}\vec{\mathcal{E}} \cdot \boldsymbol{r}_{ij}|$. Importantly, $\Omega_{\mathbf{r}, \mathbf{r}+\boldsymbol{\delta}_i^{(l)}}$ for the three $l = 1, 3$ nearest-neighbor bonds related by C_3 rotation can be different, which may lead to anisotropy terms taking the Néel vector out of the equilibrium ground-state manifold. On the other hand, for circularly polarized light, as $\text{Re}\vec{\mathcal{E}} \perp \text{Im}\vec{\mathcal{E}}$ and $|\text{Re}\vec{\mathcal{E}}| = |\text{Im}\vec{\mathcal{E}}|$, we find $\Omega_{\mathbf{r}, \mathbf{r}+\boldsymbol{\delta}_i}$ the same for $i = 1, 2, 3$. As a result, the circularly polarized pump laser could only modify the strength of the spin exchange while preserving the C_3 rotational symmetry, which may significantly modify the ground-state manifold when the equilibrium spin system is near a phase transition.

IV. APPLICATION: MAGNON DYNAMICS IN BULK NiPS₃

A. Equilibrium spin Hamiltonian

Both experimental and first-principles studies have shown that the effective spin Hamiltonian for NiPS₃ can be captured by the Heisenberg model with NN, SNN, and TNN spin exchange. As the ground-state multiplet for a Ni²⁺ ion is spin triplet and orbital singlet, the effective spin-orbit coupling (SOC) on the ground-state manifold is small, and requires mixing with higher excited levels. In the following, we express the equilibrium spin Hamiltonian as $\mathcal{H}_{\text{spin}} = \mathcal{H}_{\text{spin}}^{(0)} + \mathcal{H}_{\text{spin}}^{(1)}$, where only $\mathcal{H}_{\text{spin}}^{(1)}$ requires SOC.

The zigzag Néel order is stabilized by the isotropic Heisenberg terms [10]

$$
\mathcal{H}_{\text{spin}}^{(0)} = J_1 \sum_{\langle ij \rangle_1} \vec{S}_i \cdot \vec{S}_j + J_2 \sum_{\langle ij \rangle_2} \vec{S}_i \cdot \vec{S}_j + J_3 \sum_{\langle ij \rangle_3} \vec{S}_i \cdot \vec{S}_j \tag{25}
$$

with $\langle ij \rangle_l$ denotes the l nearest-neighbor bond, $|J_3| \gg |J_1| \gg |J_2|$, and $J_3 > 0$, $J_1 < 0$. The strength of J_3 is found at order 10 meV.

$\mathcal{H}_{\text{spin}}^{(1)}$ are generally weaker in magnitude, but they are important in the observation of coherent magnon oscillation at terahertz frequency. In the following, we model the spin anisotropy by the single-ion anisotropy [22], which reads as

$$
\mathcal{H}_{\text{spin}}^{(1)} = D_z \sum_i S_{i,z}^2 + D_{xy} \sum_i \left(S_{i,y}^2 - S_{i,x}^2\right), \tag{26}
$$

and $|D_z| \gg |D_{xy}|$. Note that with D_{3d} point-group symmetry of the crystal, only $D_z \neq 0$ is allowed. However, the bulk NiPS₃ crystalizes in a monoclinic structure [7], which breaks the threefold rotation due to displacement of adjacent layers along the $\hat{a}$ axis. This allows for a much weaker $D_{xy} \neq 0$.

In passing, we note that other anisotropic spin-exchange terms may also enter into $\mathcal{H}_{\text{spin}}^{(1)}$. However, as we discuss below, they do not modify the dynamics of slow modes qualitatively.

B. Slow modes and low-energy equation of motion

Here, we consider an easy-plane zigzag order ($D_z > 0$) which favors alignment along $\hat{x}$ ($D_{xy} > 0$). The slow modes, i.e., the Goldstone modes, are the transverse fluctuations of the Néel order, whose energy gap is determined by the the anisotropy terms in Eq. (26). When the spatial variations of the ordered state are small and slowly varying, the semiclassical spin configuration at site $\mathbf{r}$ can be described as

$$
\vec{S}_{\mathbf{r}} \equiv \vec{S}_{\mathbf{R},\alpha} = (-1)^\alpha e^{i\mathbf{M}\cdot\mathbf{R}} S\boldsymbol{n_r}\sqrt{1 - (\boldsymbol{m_r})^2} + S\boldsymbol{m_r}, \tag{27}
$$

where $\mathbf{R}$, α denote the unit-cell coordinate and sublattice label of the site $\mathbf{r}$, $\boldsymbol{n_r} = (n_0, n_y, n_z)_{\mathbf{r}}$ denotes the staggered component of the spin fields in terms of the static order parameter $n_0\hat{x}$ and transverse fluctuations $n_y\hat{y}, n_z\hat{z}$, and $\boldsymbol{m_r}$ is the ferromagnetic component of the fluctuating spin fields. The phase factor $(-1)^\alpha e^{i\mathbf{M}\cdot\mathbf{R}}$ is chosen to describe the zigzag ordering pattern (see detailed discussions in Appendix C).

We also include a general form of the *effective Hamiltonian* to model the effect of the pump field in the ultrafast regime,

$$
\mathcal{H}_{\text{eff}}^{\text{pump}} = -S(\boldsymbol{h_n} \cdot \boldsymbol{n} + \boldsymbol{h_m} \cdot \boldsymbol{m}), \tag{28}
$$

where $\boldsymbol{h_{n,m}}$ are the effective fields to be determined microscopically up to quadratic order in $|\boldsymbol{E}|^2$.

From Eqs. (25), (26), (27), and (28), we arrive at the equation of motion for the spatially homogeneous slow modes:

$$
\dot{n_y} = \chi^{-1}m_z - h_{m,z}, \quad \dot{m_z} = -\kappa_{n_y}n_y + h_{n,y};
$$
$$
\dot{n_z} = -\chi^{-1}m_y + h_{m,y}, \quad \dot{m_y} = \kappa_{n_z}n_z - h_{n,z}. \tag{29}
$$

Here, $\chi^{-1} \sim JS$ is the uniform spin susceptibility, $\kappa_{n_y}, \kappa_{n_z} \sim DS$ are the anisotropy. Note that n_y, m_z and n_z, m_y are two sets of conjugate fields. In the probe-field period, they form two sets of harmonic oscillators with frequencies $\Omega_{f_1} = \Omega_{n_y} = \sqrt{\kappa_{n_y}\chi^{-1}}$, $\Omega_{f_2} = \Omega_{n_z} = \sqrt{\kappa_{n_z}\chi^{-1}}$. In the pump period starting at $t = 0$ of duration t_p, assuming square pulses $\boldsymbol{h_{n,m}} =$

$\bar{h}_{n,m}[\Theta(t) - \Theta(t - t_p)]$, the effective magnetic fields exert forces to the spin fields, which determine the initial condition of the free oscillation in the probe period:

$$m_z(t_p^+) = \bar{h}_{n,y} t_p, \quad \partial_t m_z(t_p^+) = \kappa_{n_y} \bar{h}_{m,z} t_p;$$
$$m_y(t_p^+) = -\bar{h}_{n,z} t_p, \quad \partial_t m_z(t_p^+) = \kappa_{n_z} \bar{h}_{m,y} t_p. \quad (30)$$

C. Pump-induced effective fields and initial conditions

1. Pumping the orbital resonance

First, we discuss the initial conditions for the magnetization and the Néel vector due to the effective light-induced single-ion anisotropy. While the limit of off-resonant driving [with $t_p(\omega - \varepsilon_{m0}) \gg 1$] is readily treated in the framework presented in the previous subsection by rewriting the pump-induced effective Hamiltonian in terms of the magnetization and Néel vector continuum fields and then identifying the linear terms (with their coefficients constituting source fields), this treatment fails for driving frequencies near an orbital resonance for which the effective time evolution in the $S = 1$ ground-state sector is no longer unitary, as shown in Sec. II B. Further, we stress that the quadratic time dependence in (8) implies that a light pulse with a time-independent fluence leads to an explicit time dependence of any effective pump-induced low-energy source term, rendering the assumption leading to (30) invalid.

To mitigate this, we instead directly compute the initial conditions for the magnetization and Néel order-parameter fields through evaluating the respective time-evolved microscopic defining spin expectation values. The magnetization is given by $m_z(t_p) = \frac{1}{N} \sum_i \langle n_0 | S_i^z | n_0 \rangle (t_p)$, where the expectation value is taken with respect to the Néel reference state $|n_0\rangle = \prod_i |S^x = (-1)^{s_i} e^{i\mathbf{M} \cdot \mathbf{R}_i}\rangle_i$ corresponding to $S = 1$ moments fully polarized in the $\pm \hat{x}$ direction depending on unit-cell coordinate $\mathbf{R}_i$ and sublattice α_i of site i [see also the parametrization (27)]. Analogously, the $\hat{y}$ component of the Néel order parameter is obtained as $n_y(t_p) = \frac{1}{N} \sum_i (-1)^{\alpha_i} e^{i\mathbf{M} \cdot \mathbf{R}_i} \langle n_0 | S_i^y | n_0 \rangle (t_p)$. Using the time-evolution operator in the interaction picture, we thus find for the expectation value at site i

$$\langle n_0 | S_i^z | n_0 \rangle (t_p) = \langle \pm_i | U_{\text{eff}}^\dagger(t_p, 0) S^z U_{\text{eff}}(t_p, 0) | \pm_i \rangle. \quad (31)$$

With the general form of (13) we can write to second order

$$U_{\text{eff}}^\dagger(t_p, 0) S^z U_{\text{eff}}(t_p, 0) \approx S^z + \sum_{\mathcal{O}} \left(\text{Re}(C_{\mathcal{O}}(\mathcal{E}, \mathcal{E}^*))\{S^z, \mathcal{O}\} \right.$$
$$\left. + i \, \text{Im}(C_{\mathcal{O}}(\mathcal{E}, \mathcal{E}^*))[S^z, \mathcal{O}] \right), \quad (32)$$

where $\mathcal{O}$ denote the (products of) spin operators appearing in (13), and $C_{\mathcal{O}}(\mathcal{E})$ their respective coefficients (here, we have absorbed the electric field bilinears into the coefficients for ease of notation). We note that the nonunitarity of time evolution is reflected in the presence of the anticommutator, and unitarity is recovered in the off-resonant limit where $\text{Re} \, C_{\mathcal{O}} = 0$, as argued earlier. Taking the expectation value of (32) with respect to $|S^x = \pm\rangle$, we find that the only nonvanishing contributions are given by $\langle \{S^z, S^z\} \rangle = 1$ and $\langle [S^z, S^x S^y + S^y S^x] \rangle = -i$, as well as $\langle \pm | \{S^y, S^x S^y + S^y S^x\} | \pm \rangle = \pm 1$ and $\langle \pm | [S^z, S^z] | \pm \rangle = \pm i$. We hence find the initial conditions for the equilibrium relax-

ational dynamics of the out-of-plane magnetization and its velocity induced by the perturbation as

$$m_z(t_p^+) = \text{Re}(C_{A_2}^z) i\mathcal{E} \times \mathcal{E}^* + \text{Im}(C_E^{xy})(\mathcal{E}_x \mathcal{E}_y^* + \text{H.c.}), \quad (33a)$$
$$\partial_t m_z(t_p^+) = -\kappa n_y(t_p^+)$$
$$= -\kappa \, \text{Re}(C_E^{xy})(\mathcal{E}_x \mathcal{E}_y^* + \text{H.c.}) + \kappa \, \text{Im}(C_{A_2}^z) i\mathcal{E} \times \mathcal{E}^*, \quad (33b)$$

which supersede (30) in the regime where the coupling of the light to the orbital resonance is most dominant. We stress that Eqs. (33a) and (33b) have multiple qualitative and semiquantitative implications for experiment. Away from finite pump lengths (away from the resonant or off-resonant limits), both $C_{A_2}^z$ and C_E^{xy} are complex. Hence, by pumping with linearly or circularly polarized light the first (second) terms in (33a) and (33b) are activated and determine the initial conditions for the relaxational dynamics. By tuning ω (e.g., to the off-resonant limit such that the coefficients become purely imaginary), the balance of (33a) and (33b) is changed (and thus oscillations become more sinelike or cosinelike) in a characteristic manner, which can be observed by tracking the phase of the magnetization oscillations with respect to a fixed time $t_0 = 0$ (assuming constant pump lengths).

2. Floquet modification of spin exchange

Next, we obtain the effective magnetic field through the bond-dependent anisotropic Floquet spin Hamiltonian, which is induced by the linearly polarized pump. Note the staggered field along $\hat{z}$ and $\hat{y}$, i.e., h_{n_z} and h_{n_y}, can be obtained from $S_\mathbf{r}^x S_{\mathbf{r}+\delta_i}^z + S_\mathbf{r}^z S_{\mathbf{r}+\delta_i}^x$ and $S_\mathbf{r}^x S_{\mathbf{r}+\delta_i}^y + S_\mathbf{r}^y S_{\mathbf{r}+\delta_i}^x$ types of exchanges, respectively. To be specific, defining $J_{xz,\delta_i}^{(n)}$ as the exchange-coupling coefficient for spin bilinear $\{S^x, S^z\}$ on bond $\langle \mathbf{r}, \mathbf{r} + \delta_i \rangle$ from the nth order photon absorption, i.e., with resolvent $\frac{1}{U - n\omega}$, we find

$$\mathcal{H}_{\text{eff},n_z}^{\text{pump}} = \sum_{\mathbf{r},i} J_{xz,\delta_i}^{(1)} \left(\langle S_\mathbf{r}^x \rangle S_{\mathbf{r}+\delta_i}^z + S_\mathbf{r}^z \langle S_{\mathbf{r}+\delta_i}^x \rangle \right) + \mathcal{O}(|\vec{\mathcal{E}}|^4)$$
$$= -2S^2 n_0 \sum_{\mathbf{r},i} J_{xz,\delta_i}^{(1)} n_z$$
$$= -\frac{2S^2 n_0}{v_{\text{u.c.}}} \int d^2\mathbf{x} \left[\sum_i J_{xz,\delta_i}^{(1)} \right] n_z. \quad (34)$$

From Eqs. (24) and (34), we can read off the effective staggered magnetic field which couples to the $\hat{z}$ component of the Néel vector as

$$h_{n,z} = -2n_0 S \left[\sum_i J_{xz,\delta_i}^{(1)} \right]$$
$$= -\frac{8n_0 w_2 w_3 S}{U - \omega} \left[\left(\frac{\Omega_{\delta_1}}{\omega} \right)^2 - \frac{1}{2} \left(\frac{\Omega_{\delta_2}}{\omega} \right)^2 - \frac{1}{2} \left(\frac{\Omega_{\delta_3}}{\omega} \right)^2 \right]$$
$$= \frac{6n_0 w_2 w_3 S}{U - \omega} \left(\frac{\Omega_{\text{Rabi}}}{\omega} \right)^2 \cos 2\phi, \quad (35)$$

where $\Omega_{\mathrm{Rabi}} = e|\mathrm{Re}\vec{\mathcal{E}}||\delta_i|$. Similarly, we obtain the field for the in-plane component

$$h_{n,y} = -2n_0 S \left[\sum_i J_{xy,\delta_i}^{(1)} \right] = -\frac{3n_0 w_3^2 S}{U - \omega} \left(\frac{\Omega_{\mathrm{Rabi}}}{\omega} \right)^2 \sin 2\phi. \tag{36}$$

Using Eqs. (30) that are valid in the off-resonant limit, we can find the initial conditions for the magnetization oscillations:

$$m_z(t_p^+) \sim -\frac{w_3^2 t_p}{U - \omega} \left(\frac{\Omega_{\mathrm{Rabi}}}{\omega} \right)^2 \sin 2\phi, \quad \partial_t m_z(t_p^+) = 0;$$

$$m_y(t_p^+) \sim -\frac{w_2 w_3 t_p}{U - \omega} \left(\frac{\Omega_{\mathrm{Rabi}}}{\omega} \right)^2 \cos 2\phi, \quad \partial_t m_z(t_p^+) = 0. \tag{37}$$

D. Experimental consequences

We discuss implications from our theory to the experiment carried out by Afanasiev *et al.* in Ref. [7], where the pump beam is linearly polarized. From Eqs. (33a) and (33b), the resonant mechanism we proposed through pumping orbital resonances excites *only* the in-plane f_1 mode (i.e., out-of-plane uniform magnetization). The out-of-plane f_2 mode (i.e., in-plane uniform magnetization) cannot be excited due to the absence of the single-ion spin bilinear $\{S^x, S^z\}$ as a consequence of the orbital selection rule (see Sec. II B for detailed discussions). The amplitude of the magnetization oscillation $\bar{m}_z$ is determined by the initial conditions of $m_z(t_p^+)$ from Eqs. (33a) and (33b), and reads as

$$\bar{m}_z = \left(m_z(t_p^+)^2 + \left(\frac{\partial_t m_z(t_p^+)}{\omega} \right)^2 \right)^{1/2}$$

$$= \left(\mathrm{Im}(C_E^{xy})^2 + \frac{\kappa_{n_y}}{\chi^{-1}} \mathrm{Re}(C_E^{xy})^2 \right)^{1/2}. \tag{38}$$

Note that since $\mathrm{Im}C_E^{xy}$ and $\mathrm{Re}C_E^{xy}$ have zeros at different ω (see also Fig. 2), the above form implies that the experimentally observed amplitude does not feature zeros as a function of ω; however, in our case $\kappa/\chi^{-1} \sim D/J$ is small so that we expect the contribution from $\mathrm{Im}(C_E^{xy})$ to strongly dominate and determine the frequency dependence of $\bar{m}_z$.

From Eq. (37), the off-resonant mechanism we proposed through anisotropic Floquet spin exchange can excite both f_1 and f_2 modes. Thus, according to our theory, the observation of *only* f_2 mode in the optical transparent photon energy window $0.1 \sim 0.9$ eV implies that the hopping integrals satisfy $w_2 \gg w_3$.

We note that our theory shows that the f_1 mode can also be pumped using circularly polarized light via the orbital-resonance mechanism, according to Eqs. (33a) and (33b), constituting an example of the previously discussed inverse Faraday effect [16].

V. APPLICATION: DYNAMICS OF SPIN WAVES AND VORTICES IN MONOLAYER NiPS₃

In this section, we propose the use of pump-probe methods to study the collective dynamics spanning three distinct phases of two-dimensional XY-like magnets, arguing that the technique has the capability to observe effects associated with spin waves, vortices, and quasi-long-range order.

This possibility is built on remarkable progress made in recent years exfoliating van der Waals materials which remain magnetically ordered down to the monolayer limit [23,24]. We therefore now turn to a single (two-dimensional) layer of NiPS₃ for which recent Raman-scattering experiments find no signature of magnetic ordering in the monolayer limit [11]. Given the dominant easy-plane anisotropy in (bulk) NiPS₃ as discussed in Sec. IV, these findings suggest the intriguing possibility that the interaction between the in-plane local moments has an (approximate) SO(2) symmetry and thus monolayer NiPS₃ may realize an XY model. In two-dimensional XY models fluctuations prevent the spontaneous breaking of the SO(2) symmetry, and the model instead shows a topological phase transition at T_{BKT} from a regime with algebraically decaying correlations (at low temperatures $T < T_{\mathrm{BKT}}$) to an exponential decay (high temperatures $T > T_{\mathrm{BKT}}$) driven by the proliferation of vortices as topological defects of the order-parameter field, as shown by Berezinskii, Kosterlitz, and Thouless [25,26]. We note that surface termination effects have an impact on the precise nature and strength of interactions and anisotropies, and thus may lead to the distinct behaviors of monolayer and few-layer systems, while a naive model for the latter in terms of weakly coupled XY models would also predict the absence of long-range order. A detailed understanding requires a realistic *ab initio* modeling of the microscopic interactions which we leave for further studies.

As established experimental techniques for resolving the dynamics of magnets, e.g., neutron scattering, are only of limited applicability to 2D van der Waals magnets, the purpose of the following section is to study how the unconventional dynamics of BKT physics can be resolved within the ultrafast optical pump-probe framework outlined in Sec. I A.

We obtain a minimal action based on the above considerations by parametrizing the in-plane Néel order parameter $\boldsymbol{n} = n_0(\cos\phi, \sin\phi, 0)$ and the magnetization $\boldsymbol{m} = m_z \hat{z}$, obtaining

$$\mathcal{S}_{\mathrm{XY}} = \frac{1}{2v_{\mathrm{u.c.}}} \int dt\, d^2\boldsymbol{x} \big\{ 2Sn_0^2 m_z \partial_t \phi - \big[\rho n_0^2 (\nabla\phi)^2 + m_{\mathrm{eff}}^2 S^2 m_z^2 \big] \big\}, \tag{39}$$

where it becomes clear from the first term that the in-plane angle of the Néel order parameter ϕ and the transverse magnetization m_z are conjugate variables, for which *linear* equations of motion can be derived. $\rho \sim JS^2$ is the spin stiffness, $m_{\mathrm{eff}}^2 \sim J$ is given by the uniform spin susceptibility. We further allow for a (weak) in-plane anisotropy of strength h_p compatible with the point-group symmetry of the system (D_{3d}), which can be written as

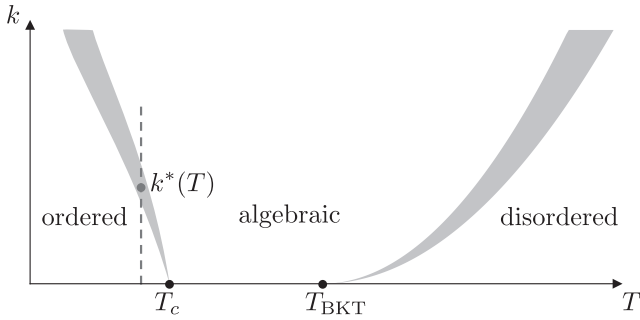$$\mathcal{S}_p = \frac{1}{2v_{\mathrm{u.c.}}} \int dt\, d^2\boldsymbol{x} \{ 2h_p \cos(p\phi) \}, \tag{40}$$

FIG. 3. Schematic illustration of the phases of the XY model with a sixfold anisotropy as a function of temperature T and at momenta k. The gray areas denote crossovers at finite momentum k. A given temperature T within the ordered phase $T < T_c$ is seen to define a critical momentum k^* above which the dynamics is well described in terms of the critical BKT scaling.

where $p = 6$ for the zigzag Néel order on the honeycomb lattice with spin-orbit coupling as discussed previously. Renormalization group studies [12] found two phase transitions, at T_{BKT} and T_c when $p = 6$, where $T_{\text{BKT}} > T_c$. Below T_c, the system orders into one of the six degenerate minima selected by the anisotropic term $\mathcal{S}_p$. Above T_{BKT}, the system is disordered with exponential decaying correlations. At any $T_c < T < T_{\text{BKT}}$, the system exhibits critical algebraic order. The phase diagram as a function of temperature (as well as scaling of excited states at finite momentum) is illustrated in Fig. 3. Following the previously described framework, we first model the pump excitation through "source" terms which couple linearly to the low-energy degrees of freedom for the duration of the pump pulse, and thus take the system out of equilibrium. The subsequent relaxational dynamics then proceeds according to the equilibrium equations of motion, with initial conditions set by demanding continuity.

A. Pump-induced effective fields

The pump-induced effective fields can be obtained by considering the bulk expression (28) restricted to the case of in-plane $\boldsymbol{n}$ and out-of-plane magnetization m_z, yielding

$$\mathcal{S}_{\text{eff}}^{\text{pump,XY}} = \frac{1}{2v_{\text{u.c.}}} \int dt\, d^2\boldsymbol{x}\, 2S[h_m m_z + n_0(h_{n,x}\cos\phi + h_{n,y}\sin\phi)]. \tag{41}$$

Here we note that the field h_m couples linearly to m_z and thus is readily incorporated as an inhomogeneity to the linear equations of motion. Using the formalism presented in Appendix D and given the (classical) correlation function $C_{m_z m_z}$ we obtain the initial conditions

$$m_z(\boldsymbol{r}, t_p^+) \simeq 0, \tag{42}$$

$$\partial_t m_z(\boldsymbol{r}, t_p^+) \simeq \int \frac{d^2k}{(2\pi)^2} h_m(\boldsymbol{k}) e^{i\boldsymbol{k}\cdot\boldsymbol{r}} \frac{\omega(k)^2 t_p}{m_{\text{eff}}^2 S}, \tag{43}$$

where $\omega(k) = \sqrt{\tilde{c}^2 k^2 + r}$ with $\tilde{c} = m_{\text{eff}}\sqrt{\rho}/n_0$ and $r = m_{\text{eff}}^2 p^2 h_p/n_0^4$. In particular, in the BKT phase, h_p is irrelevant and thus $r = 0$.

The corresponding initial conditions of the conjugate fields to m_z, ϕ, read as

$$\delta\phi(\boldsymbol{r}, t_p^+) \simeq -\int \frac{d^2\boldsymbol{k}}{(2\pi)^2} e^{i\boldsymbol{k}\cdot\boldsymbol{r}} h_m(\boldsymbol{k}) \frac{t_p}{n_0^2}, \tag{44}$$

$$\delta\partial_t\phi(\boldsymbol{r}, t_p^+) \simeq 0. \tag{45}$$

Here, we have expanded in $\omega(k)t_p \ll 1$ which corresponds to the limit of ultrafast pulses. Noting that the hydrodynamic modes in the BKT phase are described by coupled equations of m_z and $\boldsymbol{\nabla}\delta\phi$ (see later discussions in Sec. V A for details), we conclude that there is a nonvanishing response only for fields $h_m(\boldsymbol{k})$ which couple to nonzero wave vectors, i.e., are spatially nonuniform.

Contrary to h_m, the pump-induced field terms h_n lead to nonlinear inhomogeneities in the equations of motion for m_z and ϕ. To remedy this, one may be tempted to find a pump-induced initial condition linear in ϕ using linear-response theory (rather than explicitly including the inhomogeneity in the equations of motion). However, as the correlation function $\langle\phi(r',t')\cos\phi(r,t)\rangle \equiv 0$ vanishes by the (unbroken) SO(2) symmetry both above and below T_{BKT} for $h_p = 0$, we find a vanishing linear response of the phase ϕ to pump-induced effective fields $h_{n,x}$ and $h_{n,y}$.

On the other hand, if $h_p > 0$ is finite (but small compared with all other energy scales in the problem), the system orders at lowest temperatures. The low-energy excitations in this phase correspond to (gapped) fluctuations about the saddle-point field configuration of ϕ. We expand about one of the six degenerate minima of (40), $\phi_l = 2\pi l/6$ with $l = 0, \ldots, 5$, such that $\phi = \phi_l + \varepsilon\tilde{\phi}$ with $\varepsilon \ll 1$. The action for the pump-induced fields becomes (we take $l = 0$ for concreteness)

$$\mathcal{S}_{\text{eff}}^{\text{pump,XY}} = \frac{1}{2v_{\text{u.c.}}} \int dt\, d^2\boldsymbol{x}\, 2S[h_m m_z + n_0 h_{n,y}\tilde{\phi}]. \tag{46}$$

This linear coupling to the pump-induced effective fields maintains the linearity of the equations of motion and can be used to determine the initial conditions for the relaxational dynamics. We emphasize that, even though we have assumed an ordered ground state, the coupling between h_n and $\tilde{\phi}$ will excite dynamics which are of XY character if the spatial profile of $h(r)$ is sufficiently nonuniform [such as a pointlike laser irradiation yielding $h_n(r) \sim \delta(r)$]: such a field will in general couple to a broad range of momenta including both long and short wavelengths. At a given temperature, the anisotropy term h_p becomes irrelevant at short distances and accordingly excitations with large momenta become identical to those of the XY model. In the next section, a sharper criteria for the finite frequency and momentum modes that exhibit dynamics of BKT phase is presented.

For the particular case of pointlike ultrashort pulses of duration $\omega(k)t_p \ll 1$, we find the initial conditions for $\tilde{\phi}$ and its velocity (to lowest order in $t_p\omega \ll 1$)

$$\tilde{\phi}(\boldsymbol{r}, t_p^+) \simeq 0, \tag{47a}$$

$$\partial_t\tilde{\phi}(\boldsymbol{r}, t_p^+) \simeq \delta(r) \frac{m_{\text{eff}}^2 S}{n_0^3} t_p h_{n_y}, \tag{47b}$$

and correspondingly

$$\delta m_z(\boldsymbol{r}, t = t_p^+) \simeq \delta(\boldsymbol{r}) \frac{1}{n_0} t_p h_{n_y}, \tag{48a}$$

$$\delta \partial_t m_z(\boldsymbol{r}, t = t_p^+) \simeq 0, \tag{48b}$$

where we refer the reader to Appendix D for technical details.

We conclude that for all phases, i.e., below and above T_{BKT} and within the ordered phase for h_p, pump-induced fields can excite relaxational dynamics by coupling to the out-of-plane magnetization m_z. In addition, we have argued that a second (conjugate) pathway of driving spin-wave excitations with XY-model character is possible close to the transition between the vortex-paired disordered phase and the ordered phase stabilized by a weak sixfold anisotropy h_p.

B. Equations of motion and relaxation dynamics

In order to model the equilibrium dynamics of the XY model (in the absence of anisotropy and pump-induced fields), we make use of the duality between the planar XY model and $(2 + 1)$-dimensional electromagnetic U(1) gauge theory in the presence of charged matter as established by Ambegaokar, Halperin, Nelson, and Siggia (AHNS) [13] as well as Coté and Griffin [27], with the main steps reproduced by us below. The electromagnetic duality allows for a unified description of the combined dynamics of spin waves and vortices in both quasiordered and disordered phases by making use of the appropriate constitutive relations for the dual-vortex charge density and current below and above T_{BKT}.

To this end, we note that the in-plane superfluid velocity $\boldsymbol{u}_s = \boldsymbol{u}_\parallel + \boldsymbol{u}_\perp$ can be decomposed into longitudinal and transverse components which satisfy $\nabla \times \boldsymbol{u}_\parallel = 0$ and $\nabla \cdot \boldsymbol{u}_\perp = 0$. Following Refs. [13,27], these conditions may be solved by setting $\boldsymbol{u}_\parallel = \nabla f$ and $\boldsymbol{u}_\perp = \hat{z} \times \nabla g$, where f and g are some smooth differentiable functions.

The transverse component gives rise to a winding of the superfluid velocity characterized by

$$\nabla \times \boldsymbol{u}_s = 2\pi N(\boldsymbol{r}, t)\hat{z} \tag{49}$$

which defines the vortex density $N(\boldsymbol{r}, t) = \sum_i n_i \delta(\boldsymbol{r} - \boldsymbol{r}_i)$ of a collection of pointlike vortices with charges n_i at positions $\boldsymbol{r}_i$. As vortices are stable topological objects, we have the conservation law $\partial_t N + \nabla \cdot J_v = 0$ with the vortex current $J_v = \sum_i \dot{\boldsymbol{r}}_i n_i \delta(\boldsymbol{r} - \boldsymbol{r}_i)$, where $n_i = \pm 1$ is the topological charge of the ith vortex. These considerations suggest the definition of the dual electric field $\boldsymbol{e} = \boldsymbol{u}_s \times \hat{z}$, such that (49) becomes the Gauss law $\nabla \cdot \boldsymbol{e} = 2\pi N_0$.[1]

The equation of motion for m_z and ϕ from Eq. (39) gives

$$\frac{d\phi}{dt} = \frac{m_{eff}^2}{n_0^2}(Sm_z), \tag{50a}$$

$$\partial_t(Sm_z) = \rho \nabla \cdot \boldsymbol{u}_\parallel. \tag{50b}$$

Equations (50a) and (49) determine the time derivative of the superfluid velocity as

$$\partial_t \boldsymbol{u}_s = \nabla \partial_t \phi - 2\pi \hat{z} \times \boldsymbol{J}_v, \tag{51}$$

which can be rewritten as Ampère's law upon defining a magnetic field as $\boldsymbol{b} = m_{eff}/(n_0\sqrt{\rho})Sm_z\hat{z}$ (for details we refer the reader to Ref. [27]). Faraday's law follows straightforwardly from Eq. (50b), and we further have $\nabla \cdot \boldsymbol{b} = 0$ since $\boldsymbol{b} = b(x, y)\hat{z}$. The combined Maxwell equations for the gauge theory dual to the XY model thus read as

$$\nabla \cdot (\varepsilon \boldsymbol{e}) = 2\pi \varrho_v, \tag{52a}$$

$$\nabla \times \boldsymbol{e} = -\frac{1}{c_0} \frac{\partial \boldsymbol{b}}{\partial t}, \tag{52b}$$

$$\nabla \cdot \boldsymbol{b} = 0, \tag{52c}$$

$$\nabla \times \boldsymbol{b} = \frac{1}{c_0} \frac{\partial (\varepsilon \boldsymbol{e})}{\partial t} + \frac{2\pi}{c_0} \boldsymbol{J}_v, \tag{52d}$$

where $\varrho_v = N_v$ is the vortex charge density and J_v the vortex current as defined above, and $c_0 = \sqrt{\rho} m_{eff}/n_0$. We have further introduced a (so far phenomenological) dielectric constant ε to account for bound charges (see below for a detailed discussion).

It is convenient to decompose vectors in the XY plane into their longitudinal and transverse components. As introduced earlier, for the superfluid velocity we have $\boldsymbol{u}_\parallel = u_\parallel \hat{k}$ and $\boldsymbol{u}_\perp = u_\perp \hat{z} \times \hat{k}$, corresponding to spin-wave and vortex contributions, respectively. The longitudinal and transverse projections of the electric field in an analogous decomposition then read as $e_\parallel = u_\perp$ and $e_\perp = -u_\parallel$. Fourier transforming, the second Maxwell equation reads as (we write $k = |\boldsymbol{k}|$ and $\hat{k} = \boldsymbol{k}/k$)

$$ike_\perp = \frac{1}{c_0} i\omega \boldsymbol{b} \cdot \hat{z}, \tag{53}$$

making clear that the *transverse* component of the electric field couples to $\boldsymbol{b}$, i.e., Eq. (50b), such that the longitudinal components of $\boldsymbol{e}$ decouple from the equations of motion, entering only via the Gauss law $\varepsilon k e_\parallel = 2\pi \rho_v$. Combining the second and fourth Maxwell equations we finally arrive at an (inhomogeneous) wave equation for the transverse component of the electric field, written as

$$\left(\epsilon(\omega, \boldsymbol{k})\omega^2 - c_0^2 k^2\right)e_\perp(\omega, \boldsymbol{k}) = -2\pi i\omega \hat{z} \cdot (\hat{k} \times \boldsymbol{J}_v). \tag{54}$$

The solution of (54) depends on the nature of the vortex current $\boldsymbol{J}_v$ which can be related to the electric field via constitutive relations, taking different forms above and below T_{BKT}, as we detail below.

1. Gas of free vortices for $T > T_{BKT}$

Above T_{BKT}, the proliferation of vortices is entropically favored: within the electromagnetic theory described above, this phase is described in terms of a gas of free charges, with a renormalized dielectric function accounting for bound vortex-antivortex pairs with separations below a temperature-dependent characteristic separation scale $\xi_+(T)$ which diverges as $T \to T_{BKT}^+$. In order to determine the dynamics of the system, the constitutive relation for the vortex

---

[1]Note that we embed the (2+1)-dimensional electromagnetic theory into the standard (3+1)-dimensional Maxwell's equation for ease of notation; in the following we always have $\hat{z} \cdot \boldsymbol{e} = 0$ and $\boldsymbol{b} = (0, 0, b)^\top$.

current J_v must be specified. Following AHNS [13], the vortices experience a Magnus force resulting in a net transverse current as well as a stochastic force giving rise to longitudinal diffusive behavior, such that the vortex current is written

$$\boldsymbol{J}_v(\omega, k) = \gamma_0 \left(\epsilon_{ij} - D \frac{k_i k_l \epsilon_{lj}}{Dk^2 - i\omega} \right) v_j \tag{55a}$$

$$= \gamma_0 \frac{i\omega}{i\omega - Dk^2} \hat{k} e_\parallel + \gamma_0 e_\perp \hat{z} \times \hat{k}, \tag{55b}$$

where $\gamma_0 \sim Dn_f \rho^0/(k_B T) \sim \xi_+^{-2} \sim e^{-\frac{b'T}{T-T_c}}$ is a phenomenological constant and D is the diffusion constant. Using this result in (54) one arrives at

$$\left(\varepsilon_c \omega^2 + 2\pi i\omega\gamma_0 - c_0^2 k^2 \right) \boldsymbol{e}_\perp = 0. \tag{56}$$

In the limit where $c_0 k \sqrt{\varepsilon_c} \ll 2\pi \gamma_0 \sim \xi_+^{-2}$, which is applicable to all wavelengths at high temperatures and small wavelengths at successively lowered temperatures (but still $T > T_{BKT}$), it is sufficient to approximate the dielectric function by a constant $\varepsilon(k, \omega) \simeq \varepsilon_c$, as we are interested in length scales beyond the typical free vortex separation such that the $i\gamma_0\omega$ term is more important. One thus finds two modes with dispersions:

$$\omega_1^\perp = -i\frac{2\pi\gamma_0}{\varepsilon_c} \quad \text{and} \quad \omega_2^\perp = -i\frac{c_0^2 k^2}{2\pi\gamma_0}. \tag{57}$$

These modes for the transverse electric field correspond (because of $e_\perp = -u_\parallel$ and $e_\parallel = u_\parallel$) to a relaxation of the longitudinal components of the superfluid velocity. The dynamics of the longitudinal component of the electric field is obtained from the Gauss law and the continuity equation $\partial_t \varrho_v + \nabla \cdot \boldsymbol{J}_v = 0$, yielding $i\omega k e_\parallel \varepsilon = 2\pi \boldsymbol{k} \cdot \boldsymbol{J}_v$. Using $\boldsymbol{J}_v$ from above we obtain the relaxation of the longitudinal component

$$\omega^\parallel = -i\left(Dk^2 + \frac{2\pi\gamma_0}{\varepsilon_c} \right) \approx -i\frac{2\pi\gamma_0}{\varepsilon_c}. \tag{58}$$

Note that the modes $\omega_1^\perp$ and $\omega^\parallel$ are (to lowest order) independent of k and scale down to zero as $T \to T_{BKT}^+$ [13] (see Fig. 4).

2. Dielectric of vortex-antivortex pairs for $T < T_{BKT}$

Below T_{BKT}, the vortices are bound into vortex-antivortex pairs corresponding to electric dipoles in the dual electromagnetic theory, so that the free charge density $\varrho_v = 0$ and current $\boldsymbol{J}_v = 0$ vanish [13]. In this regime, the bound vortex pairs thus impact the dynamics through a (in general dynamic) renormalized dielectric function $\varepsilon(\omega)$, whose real and imaginary parts can be related to the static length-dependent dielectric function $\tilde{\varepsilon}(r)$ as $\mathrm{Re}\,\varepsilon(\omega) = \tilde{\varepsilon}(r = \sqrt{14D/\omega})$ and $\mathrm{Im}\,\varepsilon(\omega) = \pi/4r\frac{d\tilde{\varepsilon}}{dr}|_{r=\sqrt{14D/\omega}}$. After the manipulations detailed in Ref. [13], one arrives at the dispersion for the transverse electric field components (see Fig. 4)

$$\omega_\pm^\perp = \pm c_3(0)k - iD_3 k^{\pi K-1}, \tag{59}$$

where $c_3(\omega) = c_0\sqrt{\mathrm{Re}\,\varepsilon(\omega)}$ and D_3 is some constant. It thus becomes clear that in the quasiordered phase spin waves [with a linear dispersion, first term in (59)] experience damping due to the background of vortex-antivortex pairs, with a continuously varying power-law momentum dependence. Note that
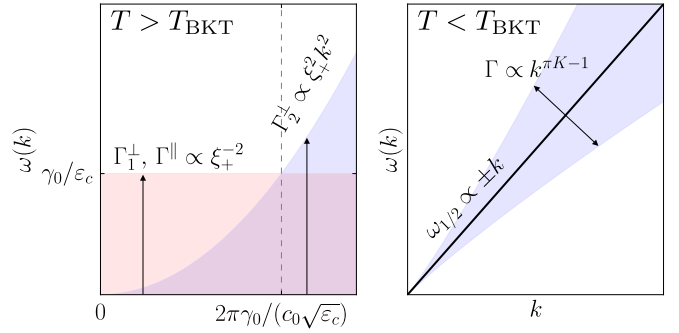

FIG. 4. Qualitative illustration of the long-wavelength dynamics of the XY model. For $T > T_{BKT}$, two decaying modes with widths $\Gamma_1^\perp$ and $\Gamma^\parallel$ as well as a diffusive mode with width $\Gamma_2^\perp$ are present, while below $T < T_{BKT}$ the dynamics is governed by two linearly dispersing spin waves with anomalous broadening. Note that the mode $\Gamma^\parallel$ corresponds to the longitudinal electric field (vortex contributions to the superfluid velocity), whose dynamics cannot be excited through the mechanisms considered here.

the absence of free charges in this regime implies that there is no dynamics of the longitudinal component of the effective electric field.

In passing, we argue that the dynamic renormalized dielectric function $\epsilon(\omega)$ discussed above applies to a wide range of frequency above $\omega^* \sim Dk^{*2}$ in the ordered phase close to the transition to BKT phase (see Fig. 5), where k^* is the crossover momentum above which the static dielectric constant $\tilde{\varepsilon}(r \sim k^{-1})$ exhibit the BKT critical power-law scaling with k, as illustrated in Fig. 3. Loosely speaking, k^* can be estimated through the static RG flow of hexagonal anisotropy h_p [12], around which the RG trajectory going towards the RG fixed point for T_c flows to the stable fixed point for ordered phase. Because the renormalization to $\epsilon(\omega)$ comes from the bound vortex-antivortex pairs separated within the distance $r_D(\omega) = \sqrt{14D/\omega}$, $\epsilon(\omega)$ is unchanged for $\omega > \omega^*$. This gives
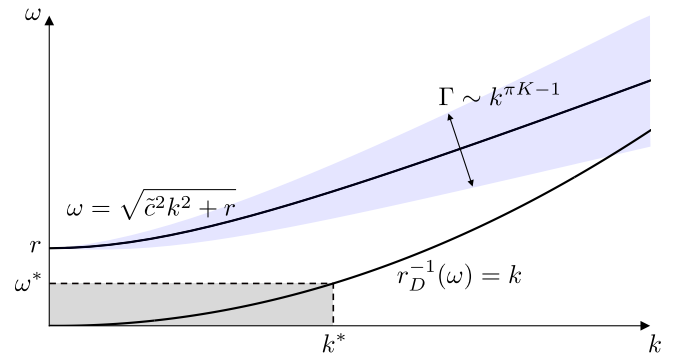

FIG. 5. Illustration of BKT scaling for excited states, i.e., the coupled transverse electric field and magnetic field, within the ordered regime. The crossover momentum k^* (see Fig. 3) determines an inverse length scale which in turn sets an energy scale ω^* [by inverting vortex-antivortex bound pair length scale $r_D(\omega)$] above which the dielectric constant receives no further corrections from h_p. Thus, the decay of the excited states exhibits BKT scaling [see Eq. (60)].

the dispersion for the transverse electric field components

$$\omega_{\pm}^{\perp} = \pm\sqrt{\tilde{c}^2 k^2 + r} - iD_3'(\tilde{c}^2 k^2 + r)^{(\pi K - 1)/2} \qquad (60)$$

for $\omega > \omega^*$. Same as in the quasiordered phase, the key difference compared with magnon mode in the conventional ordered state is the damping term due to background vortex-antivortex pairs.

C. Experimental consequences

Having formulated how the pump beam's electric field gives rise to pump-induced effective fields and modeled the low-energy dynamics of the in-plane phase and out-of-plane magnetization renormalized by the presence of free vortices or bound vortex-antivortex pairs, we briefly comment on experimental implications of our studies.

For the paramagnetic (disordered) phase above $T > T_{BKT}$, we note that no sharp quasiparticles exist, but rather only the decaying modes, two of which are momentum independent, namely, $\omega_1^{\perp}$ and $\omega^{\parallel}$. The remaining mode $\omega_2^{\perp} \sim k^2$ exhibits diffusive behavior. Note only the transverse modes $\omega^{\perp}$, which correspond to the longitudinal components of the superfluid velocity, can be excited using the microscopic mechanisms detailed earlier (this is tantamount to the fact that the probe beam does not excite free vortices). Below T_{BKT} the dynamics is given by linearly dispersing spin waves with a renormalized velocity and anomalous lifetime due to their motion in the background of vortex-antivortex pairs.

While the momentum-independent modes can in principle be probed using experimental techniques that resolve the *uniform* out-of-plane magnetization m_z (such as the magneto-optical Kerr effect), detection of the diffusive mode (and determining the diffusion constant empirically) as well as gapless spin waves (and their anomalous decay rates) would require probing the system at nonzero wave vectors. One example for such an experimental protocol is given by transient grating spectroscopy which has been successfully utilized to measure spin diffusion [28,29] and also anomalous spin propagation [30,31] in semiconductors. We further note that, as discussed in Sec. V A, highly focused pump beams (which only irradiate a small fraction of the material) couple to excitations over a broad range of momenta. Using corresponding localized probes at different positions in the material would then also allow one to probe the dynamics of excitation with nonzero wave vectors, with details depending on the nature of the experimental setup.

VI. CONCLUSION

In this work, we have established two microscopic mechanisms for driving magnetic excitations using light through the example of NiPS$_3$. While the first mechanism relies on pumping a d-d orbital resonance (which is rendered dipole allowed upon considering the inversion-symmetry-breaking S-induced crystal field in the crystal), splitting the $S = 1$ ground-state manifold via spin-orbit coupling, we have also shown that off-resonant driving can lead to a Floquet Hamiltonian with modified exchange interactions and anisotropies for the pump duration.

In a pump-probe setup, these two mechanisms will take the system out of equilibrium and set the initial conditions for the subsequent relaxational dynamics according to the low-energy (hydrodynamic) equations of motion. This work provides steps towards a more systematic understanding of the microscopic pathways how light can couple to magnetic excitations, which can be compared with experiments by studying the electric field polarization, energy, and fluence dependence of the initial condition of hydrodynamic modes set by pumping. Roles of additional (intermediate) excitations such as phonons or itinerant charge carriers will be clarified in future studies. In addition, a recent publication [32] points towards pumping coherent magnons through intermediate spin-orbital entangled exciton transition.

While the modeling of the microscopic pump mechanisms detailed above is informed by the atomic structure and nature of interactions, the relaxational dynamics (after having determined the appropriate initial conditions) depends only on the nature of the magnetic ground state and its excitations. This implies that our framework is readily applied to structurally similar compounds which can have widely differing magnetic ground states, and be used to probe their low-energy excitations. We have exemplified this by applying our framework to bulk NiPS$_3$, finding that our study can explain the recent experimental results by Afanasiev *et al.* [7]. We further suggest that pump-probe spectroscopy can be used to gain insight into monolayer NiPS$_3$ which has been found to be magnetically disordered with enhanced spin fluctuations, and thus conjectured to be a magnetic realization of the XY model, potentially realizing Berezinskii-Kosterlitz-Thouless physics, which predicts strongly renormalized dynamics due to the presence of vortex-antivortex pairs and free vortices.

We hypothesize that appropriate pump-probe setups as discussed here could be of benefit in a wide range of materials for probing and controlling intrinsic coherent magnetic excitations, in particular in few-layer (and monolayer) 2D van der Waals magnets, for which established experimental techniques such as neutron scattering are inapplicable due to sample-size limitations.

APPENDIX A: DETAILS ON SINGLE-ION CALCULATIONS

1. Explicit construction of multiplet wave functions

Here, we explicitly construct the wave functions for the A_{2g} and T_{2g} multiplets from single-particle d- and p-orbital wave

functions which we denote in the cubic basis by

$$\left|t_{2g}^{(i)}\right\rangle_{i=1,2,3} \in \{\sqrt{15}yz, \sqrt{15}zx, \sqrt{15}xy\}, \tag{A1a}$$

$$\left|e_g^{(i)}\right\rangle_{i=1,2} \in \{(3z^2 - r^2)/\sqrt{12}, (x^2 - y^2)/2\}, \tag{A1b}$$

$$\left|p^{(i)}\right\rangle_{i=1,2,3} \in \{\sqrt{3}x, \sqrt{3}y, \sqrt{3}z\}. \tag{A1c}$$

Note that the above basis states are orthonormal with respect to the inner product of spherical harmonics $\langle f|g\rangle = (4\pi)^{-1}\int_0^{2\pi}\int_0^{\pi} f^*(\phi,\theta)g(\phi,\theta)\sin\theta\,d\theta\,d\phi$. We then perform a unitary basis change to the C_3 eigenbasis with

$$U = \frac{1}{\sqrt{3}}\begin{pmatrix} 1 & \omega^2 & \omega \\ 1 & \omega & \omega^2 \\ 1 & 1 & 1 \end{pmatrix} \oplus \frac{1}{\sqrt{2}}\begin{pmatrix} 1 & 1 \\ -i & i \end{pmatrix}$$

$$\oplus \frac{1}{\sqrt{3}}\begin{pmatrix} 1 & \omega^2 & \omega \\ 1 & \omega & \omega^2 \\ 1 & 1 & 1 \end{pmatrix}, \tag{A2}$$

where $\omega = e^{i2\pi/3}$ such that the C_3 eigenstates are given by

$$(|t_1\rangle, |t_\omega\rangle, |t_{\omega^2}\rangle, |e_\omega\rangle, |e_{\omega^2}\rangle, |p_1\rangle, \dots)$$
$$= \left(\left|t_{2g}^{(1)}\right\rangle, \dots, |p^{(3)}\rangle\right)U. \tag{A3}$$

Noting that $e_g \times e_g \to {}^1A_{1g} + {}^3A_{2g}{}^{(a)} + {}^1E_g$, $e_g \times t_{2g} \to {}^1T_{1g} + {}^3T_{1g} + {}^1T_{2g} + {}^3T_{2g}$, and $t_{2g} \times t_{2g} \to {}^1A_{1g} + {}^1E_g + {}^3T_{1g}$, we can then uniquely obtain $|A_{2g}\rangle$ as given in the main text and the T_{2g} orbital triplet as

$$|T_{2g}, 1\rangle = \frac{1}{2}[|e_\omega\rangle_1 |t_{\omega^2}\rangle_2 + |e_{\omega^2}\rangle_1 |t_\omega\rangle_2 - (1 \leftrightarrow 2)],$$
$$|T_{2g}, \omega\rangle = \frac{1}{2}[|e_\omega\rangle_1 |t_1\rangle_2 + |e_{\omega^2}\rangle_1 |t_{\omega^2}\rangle_2 - (1 \leftrightarrow 2)],$$
$$|T_{2g}, \omega^2\rangle = \frac{1}{2}[|e_\omega\rangle_1 |t_\omega\rangle_2 + |e_{\omega^2}\rangle_1 |t_1\rangle_2 - (1 \leftrightarrow 2)]. \tag{A4}$$

To evaluate angular momentum L^α and dipole r^α operator matrix elements [where $r^\alpha = (x, y, z)$], we find it convenient to first evaluate them in the cubic basis and reference frame, and then change to the C_3 eigenbasis and transform into the trigonal frame using the transformation W defined by Eq. (3), such that

$$\langle d|L^\alpha|d'\rangle = \sum_{c,c'} V^{\alpha\beta} U_{dc}^\dagger \langle c|L^\beta|c'\rangle U_{c'd'}, \tag{A5}$$

and equivalently for $\langle d|r^\alpha|d'\rangle$. Here, $|c\rangle$ and $|d\rangle$ denote elements of the cubic basis and C_3 eigenbasis basis, respectively.

Evaluating the matrix elements of $L^\alpha = L_1^\alpha + L_2^\alpha$ in the subspace spanned by (A4), we obtain Eq. (2), where we identify $|l^z = +1\rangle \equiv |T_{2g}, \omega^2\rangle$, $|l^z = 0\rangle \equiv -|T_{2g}, 1\rangle$, and $|l^z = -1\rangle \equiv -|T_{2g}, \omega\rangle$.

2. Evaluation of the effective time-evolution operator

To evaluate the time-evolution operator in (7), we represent intermediate states as a linear combination $|m\rangle = V_{ls}^m |l^z\rangle |s\rangle$ where we use the shorthand $l \equiv l^z$ and $S \equiv S^z$ with some coefficients V_{ls}^m (summation convention applies). The matrix elements then follow as

$$\langle A_2|r^\alpha|m\rangle = \underbrace{\langle A_2|r^\alpha|l\rangle}_{=:M_{\alpha l}} |s\rangle V_{ls}^m = M_{\alpha l} V_{ls}^m |s\rangle. \tag{A6}$$

The matrix representation of the effective 3×3 Hamiltonian for the ground state $S = 1$ manifold then follows as

$$U_{\text{eff}} = \mathbb{1} + \sum_m \frac{(\mathcal{E}_x, \mathcal{E}_y)MV^m \otimes (V^m)^\top M^\dagger(\mathcal{E}_x^*, \mathcal{E}_y^*)^\top}{i(\omega - \varepsilon_{m0})}$$

$$\times \left[t_p - \frac{e^{i(\omega - \varepsilon_{m0})t_p} - 1}{i(\omega - \varepsilon_{m0})}\right], \tag{A7}$$

where "$\otimes$" denotes the outer (dyadic) product. We decompose $\mathcal{U}_{\text{eff}} \sim \sum_{\mathcal{O}} C_{\mathcal{O}} \mathcal{O}$ into a basis of 3×3 Hermitian operators $\mathcal{O}$ by taking the operator scalar product $C_{\mathcal{O}} = \text{tr}[\mathcal{H}_{\text{eff}} \mathcal{O}]/2$ where $\mathcal{O} \in \{\mathbb{1}, S^\alpha, \{S^\alpha, S^\beta\}, (S^x)^2 - (S^y)^2, (3(S^z)^2 - 2\mathbb{1})/\sqrt{3}\}$ with $\alpha < \beta$.

APPENDIX B: DETAILS ON SPIN-EXCHANGE CALCULATIONS

Useful expressions

The threefold rotation along $\hat{z}$ in trigonal coordinate on fermion basis Ψ and $3d$ vectors, respectively, are

$$W_{C_3} = e^{i\frac{2\pi}{3}\tau_y} \otimes_{\text{Kron}} e^{i\frac{\pi}{3}\sigma_z} \quad \text{and} \quad \mathcal{R}_{C_3} = \begin{pmatrix} -\frac{1}{2} & \frac{\sqrt{3}}{2} & 0 \\ \frac{\sqrt{3}}{2} & -\frac{1}{2} & 0 \\ 0 & 0 & 1 \end{pmatrix}. \tag{B1}$$

From Eqs. (19), (20), and (B1), the equilibrium spin-exchange interaction on bonds $\boldsymbol{\delta}_{2,3}$ can be expressed explicitly as

$$\Gamma^{\delta_2} = \begin{pmatrix} J_l - J_l' - \frac{1}{2}J_l'' & \frac{\sqrt{3}}{2}J_l'' & -\frac{1}{2}J_{l,xz} \\ \frac{\sqrt{3}}{2}J_l'' & J_l - J_l' + \frac{1}{2}J_l'' & -\frac{\sqrt{3}}{2}J_{l,xz} \\ -\frac{1}{2}J_{l,xz} & -\frac{\sqrt{3}}{2}J_{l,xz} & J_l + J_l' - J_l'' \end{pmatrix},$$

$$\Gamma^{\delta_3} = \begin{pmatrix} J_l - J_l' - \frac{1}{2}J_l'' & -\frac{\sqrt{3}}{2}J_l'' & -\frac{1}{2}J_{l,xz} \\ -\frac{\sqrt{3}}{2}J_l'' & J_l - J_l' + \frac{1}{2}J_l'' & \frac{\sqrt{3}}{2}J_{l,xz} \\ -\frac{1}{2}J_{l,xz} & \frac{\sqrt{3}}{2}J_{l,xz} & J_l + J_l' - J_l'' \end{pmatrix}, \tag{B2}$$

where $l = 1, 3$ refers to NN and TNN couplings.

APPENDIX C: EQUATION OF MOTION FOR LOW-ENERGY SPIN FIELDS

Here, we derive the equation of motion (EoM) for the low-energy spin fields. We will consider both the duration of the pump field and the probe period. We proceed with the standard nonlinear sigma model (NLSM) formulation for collinear antiferromagnets, and obtain the effective Lagrangian in terms of the continuous spin fields, i.e., the staggered fields ($\boldsymbol{n}$), their conjugate ferromagnetic fields ($\boldsymbol{m}$). To model the effects of the pump field, we further consider the effective magnetic field $\boldsymbol{h}_n, \boldsymbol{h}_m$ that couples to $\boldsymbol{n}, \boldsymbol{m}$, respectively.

Following Ref. [33], the coherent state path integral for a Heisenberg spin with spin value S at site $\mathbf{r}$ can be obtained in the basis of the (unit) vector field $\boldsymbol{e}_\mathbf{r}$, which is defined through $\hat{\mathbf{S}}_\mathbf{r}|\boldsymbol{e}_\mathbf{r}\rangle = S\boldsymbol{e}_\mathbf{r}|\boldsymbol{e}_\mathbf{r}\rangle$ and $|\boldsymbol{e}_\mathbf{r}|^2 = 1$. For a collinear zigzag Néel order, it is convenient to parametrize $\boldsymbol{e}_\mathbf{r}$ as

$$\boldsymbol{e}_\mathbf{r} \equiv \boldsymbol{e}_{\mathbf{R},\alpha} = (-1)^\alpha e^{i\mathbf{M}\cdot\mathbf{R}} \boldsymbol{n}_\mathbf{r}\sqrt{1 - (\boldsymbol{m}_\mathbf{r})^2} + \boldsymbol{m}_\mathbf{r}, \tag{C1}$$

where $\mathbf{M}$ is the wave vector of the zigzag order, $\boldsymbol{n}$ is the staggered component with normalization condition $|\boldsymbol{n}| = 1$, $\boldsymbol{m}$ is the uniform magnetization per site in unit of the saturation magnetization ($= S$ semiclassically). We have defined $\mathbf{r} = \mathbf{R} + \boldsymbol{u}_\alpha$, where $\mathbf{R}$ is the coordinate of a unit cell, α labels the A and B sublattices on a honeycomb lattice. Without loss of generality, we consider the zigzag order with $\boldsymbol{M} = (0, \frac{2\pi}{\sqrt{3}})$, and $\boldsymbol{u}_A = 0$, $\boldsymbol{u}_B = (0, -\frac{1}{\sqrt{3}})$.

The effective spin action for the spin Hamiltonian $\mathcal{H}_{\text{spin}}$ is

$$
\mathcal{Z}_s = \int \mathcal{D}\boldsymbol{n}\,\mathcal{D}\boldsymbol{m}\,\delta(\boldsymbol{n}^2 - 1)\delta(\boldsymbol{n}\cdot\boldsymbol{m})\exp(i\mathcal{S}_s),
$$

$$
\mathcal{S}_s = \frac{1}{2\upsilon_{\text{u.c.}}}\int dx\,dy\,dt \left\{ 2S\boldsymbol{m}\cdot\left(\boldsymbol{n}\times\frac{\partial\boldsymbol{n}}{\partial t}\right) - m_{\text{eff}}^2 S^2 \boldsymbol{m}^2 \right.
$$
$$
- 4(D_z + D_{xy})S^2 n_z^2 - 8D_{xy}S^2 n_y^2 + \rho\upsilon_{\text{u.c.}}(\boldsymbol{\nabla}\boldsymbol{n})^2
$$
$$
\left. + 2S(\boldsymbol{h}_n\cdot\boldsymbol{n} + \boldsymbol{h}_m\cdot\boldsymbol{m}) \right\}, \tag{C2}
$$

where $\upsilon_{\text{u.c.}}$ is the volume of the unit cell, coming from converting $\frac{1}{2}\sum_{\mathbf{r}} \to \frac{1}{\upsilon_{\text{u.c.}}}\int dx\,dy$, with the factor $\frac{1}{2}$ entering due to two-sublattice unit cell $m_{\text{eff}}^2 = 4(J_1 + 3J_3)$.

To study the homogeneous order-parameter dynamics, the spatial gradient on $\boldsymbol{n}, \boldsymbol{m}$ can be ignored. Below, we consider a zigzag order with the Néel vector along the x axis, i.e., $\lim_{h\to0}\langle\boldsymbol{n}\rangle = n_0\hat{\boldsymbol{x}}$. The staggered field can be parametrized by $\boldsymbol{n} = \{n_0, n_y, n_z\}$, where $n_0 = \sqrt{1 - n_y^2 - n_z^2}$ is the order parameter, and $n_{y,z}$ are transverse fluctuations (spin waves). The first term in $\mathcal{S}_s$ comes from the Berry phase of a quantum spin operator, and in terms of $n_{y,z}$ and $m_{y,z}$, it becomes

$$
2S\boldsymbol{m}\cdot\left(\boldsymbol{n}\times\frac{\partial\boldsymbol{n}}{\partial t}\right) \longrightarrow -2Sn_0(m_y\partial_t n_z - m_z\partial_t n_y), \tag{C3}
$$

which indicates that n_y, m_z and n_z, m_y are two sets of conjugate fields. Applying the Euler-Lagrange equation for n_y, m_z and n_z, m_y, we arrived at the EoM for the continuous fields

$$
\dot{n}_y = \chi^{-1}m_z - h_{m,z}, \quad \dot{m}_z = -8SD_{xy}n_y + h_{n,y},
$$
$$
\dot{n}_z = -\chi^{-1}m_y + h_{m,y}, \quad \dot{m}_y = 4S(D_z + D_{xy})n_z - h_{n,z}. \tag{C4}
$$

Here, χ is the uniform spin susceptibility, at the leading order in $1/S$ and ignoring the anisotropy, it is determined by $\chi_0^{-1} = Sm_{\text{eff}}^2/n_0 = 4S(J_1 + 3J_3)/n_0$.

Equation (C4) can be further expressed as

$$
\partial_t^2 m_z + 2\gamma\partial_t m_z + \Omega_{n_y}^2 m_z = \kappa_{n_y}h_{m,z} + \partial_t h_{n,y},
$$
$$
\partial_t^2 m_y + 2\gamma\partial_t m_y + \Omega_{n_z}^2 m_y = \kappa_{n_z}h_{m,y} - \partial_t h_{n,z}. \tag{C5}
$$

Here, we have introduced a phenomenological decay term with decay rate γ, which physically comes from coupling with the environment and satisfies the causality. The oscillation frequencies are $\Omega_{f_1} = \Omega_{n_y} = \sqrt{8SD_{xy}\chi^{-1}} = 2S\sqrt{2(J_1 + 3J_3)D_{xy}}$, $\Omega_{f_2} = \Omega_{n_z} = \sqrt{4S(D_z + D_{xy})\chi^{-1}} = 2S\sqrt{(J_1 + 3J_3)(D_z + D_{xy})}$.

APPENDIX D: INITIAL CONDITIONS IN LINEAR-RESPONSE THEORY

The initial conditions for the relaxational dynamics (according to the equilibrium equations of motions) due to the effective pump-induced fields can be computed in linear-response theory. Here we consider the pump-induced Hamiltonian of a field $h_\mathcal{O}$ coupling to the (classical) observable $\mathcal{O}$ with $\mathcal{H}^{\text{pump}} = -(2\upsilon_{\text{u.c.}})^{-1}\int dt\,d^2r\,h_\mathcal{O}(t, \boldsymbol{r})\mathcal{O}(t, \boldsymbol{r})$. We are interested in the response of $\mathcal{O}'$ due to the pump field $h_\mathcal{O}$, noting that $\mathcal{O}$ and $\mathcal{O}'$ are not necessarily the same. Hereafter, we assume that $\langle\mathcal{O}'\rangle = 0$ in equilibrium. The linear response of the observable $\mathcal{O}'$ is then given by

$$
\delta\mathcal{O}'(\boldsymbol{r}, t) = (2\upsilon_{\text{u.c.}})^{-1}\int d^2r'\int_{-\infty}^{\infty}dt'\chi_{\mathcal{O}'\mathcal{O}}(\boldsymbol{r} - \boldsymbol{r}', t - t')
$$
$$
\times h_\mathcal{O}(\boldsymbol{r}', t'), \tag{D1}
$$

where $\chi_{\mathcal{O}'\mathcal{O}}(\boldsymbol{r}, t)$ is the susceptibility (retarded response function) of $\mathcal{O}'$ and $\mathcal{O}$. We assume a "box" temporal pump profile of the form $h_\mathcal{O}(r, t) = \bar{h}_\mathcal{O}(r)[\Theta(t) - \Theta(t - t_p)]$, where t_p is the pump duration and $\bar{h}_\mathcal{O}(r)$ is the (in general spatially dependent) pump strength. We evaluate the initial conditions shortly after the pump pulse at time $t = t_p^+$ such that $t_p^+ - t_p = 0^+$ is an infinitesimally small positive number, yielding $\delta\mathcal{O}'|_{t=t_p^+} = (2\upsilon_{\text{u.c.}})^{-1}\int d^2r\int_0^{t_p}dt'\bar{h}_\mathcal{O}(\boldsymbol{r}')\chi(\boldsymbol{r} - \boldsymbol{r}', t_p^+ - t')$ and similarly for $\partial_t\delta\mathcal{O}$. For brevity, the subscript of χ will be dropped unless there is ambiguity. Writing the susceptibility in terms of its imaginary part $\chi''(\omega)$ in the frequency domain $\chi(t - t') = \int d\omega'\frac{i}{\pi}e^{-i\omega(t-t')}\chi''(\omega)\Theta(t - t')$ (which is obtained making use of Kramers-Kronig relations and Plemelji theorem) [34], the temporal integration can be performed,

$$
\delta\mathcal{O}'|_{t=t_p^+} = (2\upsilon_{\text{u.c.}})^{-1}\int d^2r'\int d\omega'h_\mathcal{O}(\boldsymbol{r}')\frac{1}{\pi\omega'}(1 - e^{-it_p\omega'})
$$
$$
\times \chi''(\boldsymbol{r} - \boldsymbol{r}', \omega'). \tag{D2}
$$

We further note that χ'' is related to the correlation function $C_{\mathcal{O}'\mathcal{O}}(\boldsymbol{r}, t) = \langle\mathcal{O}'(\boldsymbol{r}, t)\mathcal{O}(0, 0)\rangle$ through the fluctuation-dissipation theorem. In the classical limit it reads as $2\chi''(\omega, \boldsymbol{k}) = \beta\omega C(\omega, \boldsymbol{k})$, thus

$$
\delta\mathcal{O}'|_{t=t_p^+}(\boldsymbol{r}) = (2\upsilon_{\text{u.c.}})^{-1}\int\frac{d^2k}{(2\pi)^2}\int d\omega'\frac{\beta}{2\pi}e^{i\boldsymbol{k}\cdot\boldsymbol{r}}(1 - e^{-it_p\omega'})
$$
$$
\times \bar{h}_\mathcal{O}(\boldsymbol{k})C(\omega', \boldsymbol{k}). \tag{D3}
$$

Depending on the nature of perturbing and responding observables, it is convenient to use either Eq. (D1), (D2), or (D3). To proceed, it is convenient to relate the response function $\chi_{(\partial_t\mathcal{O}')\mathcal{O}}$ and $\chi_{\mathcal{O}'(\partial_t\mathcal{O})}$ with $\chi_{\mathcal{O}'\mathcal{O}}$ as

$$
\chi_{(\partial_t\mathcal{O}')\mathcal{O}}(\omega, \boldsymbol{k}) = -\chi_{\mathcal{O}'(\partial_t\mathcal{O})}(\omega, \boldsymbol{k}) = \frac{\omega}{i}\chi_{\mathcal{O}'\mathcal{O}}(\omega, \boldsymbol{k}), \tag{D4}
$$

where using $\chi_{(\partial_t\mathcal{O}')\mathcal{O}}$ in the linear-response formulas above gives the initial condition of $\delta\partial_t\mathcal{O}'$.

1. Linear response deep in the ordered state

To obtain the initial condition in the probe period for coherent magnon in the zigzag-ordered state, we follow the discussion in Ref. [6], from Eq. (C5), the Fourier transform of

spin susceptibility at $\boldsymbol{k} = 0$ reads as

$$\chi_{m_z m_z}(\omega) \sim \frac{1}{\omega^2 + 2i\gamma\omega - \Omega_{n_y}^2}. \tag{D5}$$

In the limit of short pulse, i.e., $t_p \ll \omega^{-1}, \gamma^{-1}$, the effective field $\boldsymbol{h}_m$ acts as an impulse to the magnetization, giving the magnetization an initial velocity $\partial_t m$, while the effective field $\boldsymbol{h}_n$ provides initial amplitude of $\boldsymbol{m}$ for free oscillation in the probe period. We find (setting $n_0 \equiv 1$)

$$m_z(t_p^+) = \bar{h}_{n,y} t_p, \quad \partial_t m_z(t_p^+) = \kappa_{n_y} \bar{h}_{m,z} t_p,$$
$$m_y(t_p^+) = -\bar{h}_{n,z} t_p, \quad \partial_t m_z(t_p^+) = \kappa_{n_z} \bar{h}_{m,y} t_p. \tag{D6}$$

2. Linear response in and proximate to the BKT phase

In and proximate to the BKT phase, it is convenient to describe the dynamics in terms of the magnetization field m_z and the phase field ϕ, which can be conveniently formulated in terms of a dual electromagnetic theory. Defining $\phi = \phi_{l=0} + \tilde{\phi}$ (without loss of generality, we take $\phi_l = 0$), the action for the XY model with hexagonal anisotropy h_p after integrating out m_z and performing the saddle-point expansion about $\phi_{l=0} = 0$ reads as

$$S_{XY} = \frac{1}{2v_{u.c.}} \int dt\, d^2\boldsymbol{x} \left[\frac{n_0^4}{m_{eff}^2}(\partial_t \tilde{\phi})^2 - \rho n_0^2 (\nabla \tilde{\phi})^2 - h_p p^2 \tilde{\phi}^2 \right]. \tag{D7}$$

The classical correlation function (i.e., assuming that the mode is on shell only) is obtained as

$$C_{\tilde{\phi}\tilde{\phi}}(\boldsymbol{k}, \omega) = \frac{\pi m_{eff}^2 v_{u.c.}}{\beta n_0^4 \omega(k)^2} [\delta[\omega - \omega(k)] + \delta[\omega + \omega(k)]], \tag{D8}$$

where $\omega(k) = \sqrt{\tilde{c}^2 k^2 + r}$ with $\tilde{c} = m_{eff}\sqrt{\rho}/n_0$ and $r = m_{eff}^2 p^2 h_p/n_0^4$, with $\beta^{-1} = k_B T$ as usual. In particular, in the BKT phase, h_p is irrelevant and thus $r = 0$.

The autocorrelation function for the conjugate field m_z reads as

$$C_{m_z m_z}(\boldsymbol{k}, \omega) = \frac{\pi v_{u.c.}}{\beta m_{eff}^2 S^2} [\delta[\omega - \omega(k)] + \delta[\omega + \omega(k)]]. \tag{D9}$$

From $\mathcal{S}_{eff}^{pump,XY}$ we read off $\bar{h}_{m_z} = 2Sh_m$ and thus obtain

$$\delta m_z(\boldsymbol{r}, t_p^+) = \int \frac{d^2\boldsymbol{k}}{(2\pi)^2} e^{i\boldsymbol{k}\cdot\boldsymbol{r}} h_m(\boldsymbol{k}) \frac{1}{m_{eff}^2 S} \{1 - \cos[\omega(k)t_p]\}, \tag{D10a}$$

$$\delta\partial_t m_z(\boldsymbol{r}, t_p^+) = \int \frac{d^2\boldsymbol{k}}{(2\pi)^2} e^{i\boldsymbol{k}\cdot\boldsymbol{r}} h_m(\boldsymbol{k}) \frac{1}{m_{eff}^2 S} \omega(k) \sin[\omega(k)t_p]. \tag{D10b}$$

Using the autocorrelation for ϕ fields from Eqs. (D8) and (D4), the initial condition for the phase field $\delta\phi(\boldsymbol{r}, t_p^+)$ reads as

$$\delta\phi(\boldsymbol{r}, t_p^+) = -\int \frac{d^2\boldsymbol{k}}{(2\pi)^2} e^{i\boldsymbol{k}\cdot\boldsymbol{r}} h_m(\boldsymbol{k}) \frac{1}{n_0^2 \omega(k)} \sin[\omega(k)t_p], \tag{D11a}$$

$$\delta\partial_t\phi(\boldsymbol{r}, t_p^+) = \int \frac{d^2\boldsymbol{k}}{(2\pi)^2} e^{i\boldsymbol{k}\cdot\boldsymbol{r}} h_m(\boldsymbol{k}) \frac{1}{n_0^2} \{1 - \cos[\omega(k)t_p]\}. \tag{D11b}$$

In the limit $t_p \omega(k) \ll 1$, the initial conditions read as

$$\delta m_z(\boldsymbol{k}, t_p^+) \approx 0, \quad \delta\partial_t m_z(\boldsymbol{k}, t_p^+) \approx \frac{\omega(k)^2}{m_{eff}^2 S} h_m t_p, \tag{D12a}$$

$$\delta\phi(\boldsymbol{k}, t_p^+) \approx -\frac{1}{n_0^2} h_m t_p, \quad \delta\partial_t\phi(\boldsymbol{k}, t_p^+) \approx 0. \tag{D12b}$$

In the ordered phase due to the relevant sixfold hexagonal anisotropy perturbation h_p, it is argued in the main text that the pump-induced field $\boldsymbol{h}_n$ may also induce hydrodynamic modes of the BKT phase at finite wave vector when T is close to T_c. Further, with $\bar{h}_{\tilde{\phi}} = 2Sn_0 h_{n_y}$ and assuming a $\delta(\boldsymbol{r})$-spatial profile of the pump-induced fields, we obtain using $C_{\tilde{\phi}\tilde{\phi}}$ from (D8), after performing the ω' integration,

$$\delta\tilde{\phi}(\boldsymbol{r}, t = t_p^+) = \int \frac{d^2\boldsymbol{k}}{(2\pi)^2} e^{i\boldsymbol{k}\cdot\boldsymbol{r}} h_{n_y}(\boldsymbol{k}) \frac{S m_{eff}^2}{n_0^3 \omega(k)^2} \{1 - \cos[\omega(k)t_p]\}, \tag{D13a}$$

$$\delta\partial_t\tilde{\phi}(\boldsymbol{r}, t = t_p^+) = \int \frac{d^2\boldsymbol{k}}{(2\pi)^2} e^{i\boldsymbol{k}\cdot\boldsymbol{r}} h_{n_y}(\boldsymbol{k}) \frac{S m_{eff}^2}{n_0^3 \omega(k)} \sin[t_p \omega(k)] \tag{D13b}$$

and

$$\delta m_z(\boldsymbol{r}, t = t_p^+) = \int \frac{d^2\boldsymbol{k}}{(2\pi)^2} e^{i\boldsymbol{k}\cdot\boldsymbol{r}} h_{n_y}(\boldsymbol{k}) \frac{1}{n_0 \omega(k)} \sin[t_p \omega(k)], \tag{D14a}$$

$$\delta\partial_t m_z(\boldsymbol{r}, t = t_p^+) = \int \frac{d^2\boldsymbol{k}}{(2\pi)^2} e^{i\boldsymbol{k}\cdot\boldsymbol{r}} h_{n_y}(\boldsymbol{k}) \frac{1}{n_0} \{1 - \cos[\omega(k)t_p]\}, \tag{D14b}$$

where $\omega(k) = \sqrt{\tilde{c}^2 k^2 + r}$, with r the hexagonal anisotropy gap. Expanding in $t_p \omega(k) \ll 1$ then leads to Eqs. (47a) and (47b).

[1] A. Kirilyuk, A. V. Kimel, and T. Rasing, Rev. Mod. Phys. **82**, 2731 (2010).

[2] D. N. Basov, R. D. Averitt, and D. Hsieh, Nat. Mater. **16**, 1077 (2017).

[3] A. de la Torre, D. M. Kennes, M. Claassen, S. Gerber, J. W. McIver, and M. A. Sentef, Rev. Mod. Phys. **93**, 041002 (2021).

[4] N. P. Duong, T. Satoh, and M. Fiebig, Phys. Rev. Lett. **93**, 117402 (2004).

[5] C. Tzschaschel, K. Otani, R. Iida, T. Shimura, H. Ueda, S. Günther, M. Fiebig, and T. Satoh, Phys. Rev. B **95**, 174407 (2017).

[6] U. F. P. Seifert and L. Balents, Phys. Rev. B **100**, 125161 (2019).

[7] D. Afanasiev, J. R. Hortensius, M. Matthiesen, S. Mañas-Valero, M. Šiškins, M. Lee, E. Lesne, H. S. J. van der Zant, P. G. Steeneken, B. A. Ivanov, E. Coronado, and A. D. Caviglia, Sci. Adv. **7**, eabf3096 (2021).

[8] A. R. Wildes, V. Simonet, E. Ressouche, G. J. McIntyre, M. Avdeev, E. Suard, S. A. J. Kimber, D. Lançon, G. Pepe, B. Moubaraki, and T. J. Hicks, Phys. Rev. B **92**, 224408 (2015).

[9] D. Lançon, R. A. Ewings, T. Guidi, F. Formisano, and A. R. Wildes, Phys. Rev. B **98**, 134414 (2018).

[10] Y. Gu, Q. Zhang, C. Le, Y. Li, T. Xiang, and J. Hu, Phys. Rev. B **100**, 165405 (2019).

[11] K. Kim, S. Y. Lim, J.-U. Lee, S. Lee, T. Y. Kim, K. Park, G. S. Jeon, C.-H. Park, J.-G. Park, and H. Cheong, Nat. Commun. **10**, 345 (2019).

[12] J. V. José, L. P. Kadanoff, S. Kirkpatrick, and D. R. Nelson, Phys. Rev. B **16**, 1217 (1977).

[13] V. Ambegaokar, B. I. Halperin, D. R. Nelson, and E. D. Siggia, Phys. Rev. B **21**, 1806 (1980).

[14] E. M. Stoudenmire, S. Trebst, and L. Balents, Phys. Rev. B **79**, 214436 (2009).

[15] J. P. van der Ziel, P. S. Pershan, and L. D. Malmstrom, Phys. Rev. Lett. **15**, 190 (1965).

[16] P. S. Pershan, J. P. van der Ziel, and L. D. Malmstrom, Phys. Rev. **143**, 574 (1966).

[17] S. Y. Kim, T. Y. Kim, L. J. Sandilands, S. Sinn, M.-C. Lee, J. Son, S. Lee, K.-Y. Choi, W. Kim, B.-G. Park, C. Jeon, H.-D. Kim, C.-H. Park, J.-G. Park, S. J. Moon, and T. W. Noh, Phys. Rev. Lett. **120**, 136402 (2018).

[18] S. Kang, K. Kim, B. H. Kim, J. Kim, K. I. Sim, J.-U. Lee, S. Lee, K. Park, S. Yun, T. Kim, A. Nag, A. Walters, M. Garcia-Fernandez, J. Li, L. Chapon, K.-J. Zhou, Y.-W. Son, J. H. Kim, H. Cheong, and J.-G. Park, Nature (London) **583**, 785 (2020).

[19] G. Le Flem, R. Brec, G. Ouvard, A. Louisy, and P. Segransan, J. Phys. Chem. Solids **43**, 455 (1982).

[20] S. Chaudhary, A. Ron, D. Hsieh, and G. Refael, arXiv:2009.00813.

[21] K. Hejazi, J. Liu, and L. Balents, Phys. Rev. B **99**, 205111 (2019).

[22] P. A. Joy and S. Vasudevan, Phys. Rev. B **46**, 5425 (1992).

[23] K. F. Mak, J. Shan, and D. C. Ralph, Nat. Rev. Phys. **1**, 646 (2019).

[24] M. Gibertini, M. Koperski, A. F. Morpurgo, and K. S. Novoselov, Nat. Nanotechnol. **14**, 408 (2019).

[25] V. L. Berezinsky, Zh. Eksp. Teor. Fiz. **59**, 907 (1970) [Sov. Phys.–JETP **32**, 493 (1971)].

[26] J. M. Kosterlitz and D. J. Thouless, J. Phys. C: Solid State Phys. **6**, 1181 (1973).

[27] R. Cté and A. Griffin, Phys. Rev. B **34**, 6240 (1986).

[28] A. R. Cameron, P. Riblet, and A. Miller, Phys. Rev. Lett. **76**, 4793 (1996).

[29] C. P. Weber, N. Gedik, J. E. Moore, J. Orenstein, J. Stephens, and D. D. Awshalom, Nature (London) **437**, 1330 (2005).

[30] C. P. Weber, J. Orenstein, B. A. Bernevig, S.-C. Zhang, J. Stephens, and D. D. Awshalom, Phys. Rev. Lett. **98**, 076604 (2007).

[31] J. D. Koralek, C. P. Weber, J. Orenstein, B. A. Bernevig, S.-C. Zhang, S. Mack, and D. D. Awshalom, Nature (London) **458**, 610 (2009).

[32] C. A. Belvin, E. Baldini, I. Ozge Ozel, D. Mao, H. C. Po, C. J. Allington, S. Son, B. H. Kim, J. Kim, I. Hwang, J. H. Kim, J.-G. Park, T. Senthil, and N. Gedik, Nat. Commun. **12**, 4837 (2021).

[33] S. Sachdev, *Quantum Phase Transitions* (Cambridge University Press, Cambridge, 2009).

[34] P. Coleman, *Introduction to Many-Body Physics* (Cambridge University Press, Cambridge, 2015).